

The Architecture of the Multisubunit TRAPP I Complex Suggests a Model for Vesicle Tethering

Yeon-Gil Kim,¹ Stefan Raunser,² Christine Munger,³ John Wagner,⁴ Young-Lan Song,¹ Mirosław Cygler,⁴ Thomas Walz,² Byung-Ha Oh,^{1,*} and Michael Sacher^{5,*}

¹Center for Biomolecular Recognition and Division of Molecular and Life Sciences, Department of Life Sciences, Pohang University of Science and Technology, Pohang, Kyungbuk 790-784, South Korea

²Department of Cell Biology, Harvard Medical School, 240 Longwood Avenue, Boston, MA 02115, USA

³Department of Biochemistry, McGill University, 3655 Drummond, Montreal, Quebec H3G 1Y6, Canada

⁴Biotechnology Research Institute, 6100 Royalmount Avenue, Montreal, Quebec H4P 2R2, Canada

⁵Department of Biology, Concordia University, 7141 Sherbrooke Street West, Montreal, Quebec H4B 1R6, Canada

*Contact: bhoh@postech.ac.kr (B.-H.O.), msacher@alcor.concordia.ca (M.S.)

DOI 10.1016/j.cell.2006.09.029

SUMMARY

Transport protein particle (TRAPP) I is a multisubunit vesicle tethering factor composed of seven subunits involved in ER-to-Golgi trafficking. The functional mechanism of the complex and how the subunits interact to form a functional unit are unknown. Here, we have used a multidisciplinary approach that includes X-ray crystallography, electron microscopy, biochemistry, and yeast genetics to elucidate the architecture of TRAPP I. The complex is organized through lateral juxtaposition of the subunits into a flat and elongated particle. We have also localized the site of guanine nucleotide exchange activity to a highly conserved surface encompassing several subunits. We propose that TRAPP I attaches to Golgi membranes with its large flat surface containing many highly conserved residues and forms a platform for protein-protein interactions. This study provides the most comprehensive view of a multisubunit vesicle tethering complex to date, based on which a model for the function of this complex, involving Rab1-GTP and long, coiled-coil tethers, is presented.

INTRODUCTION

In eukaryotic cells, movement of proteins between different subcellular compartments is a highly regulated process mediated by many different factors, including SNAREs and SNARE attachment proteins (Gerst, 1999), small GTP-binding proteins (Pfeffer, 1996), and vesicle tethering factors (Whyte and Munro, 2002). Tethering factors can be categorized as long, coiled-coil proteins (e.g.,

p115, Uso1p, and GM130/golgin-95) or multisubunit protein complexes that physically link the vesicles and the target membranes upstream of membrane fusion and are believed to significantly contribute to the specificity of the transport reaction (Lowe, 2000; Whyte and Munro, 2002). How the different types of tethering factors contribute to the overall specificity of this process is presently unknown.

Transport protein particle (TRAPP) complexes I and II are required for tethering endoplasmic reticulum (ER)-derived vesicles to Golgi membranes and for Golgi traffic (Cai et al., 2005; Sacher et al., 1998, 2001). The complexes localize to the Golgi compartment, where they recognize and capture transport vesicles destined to fuse with this organelle (Sacher et al., 1998, 2001). The yeast TRAPP I complex consists of seven different proteins (Bet5p, Bet3p, Trs20p, Trs23p, Trs31p, Trs33p, and Trs85p), while TRAPP II contains three additional subunits (Trs65p, Trs120p, and Trs130p). The mechanism by which the TRAPP complexes mediate the tethering process is unknown, although in yeast, it may involve the exchange of guanine nucleotide on Ypt1p, a Rab GTPase family member (Jones et al., 2000; Wang et al., 2000).

The structures and functions of the TRAPP subunits are being elucidated. The structure of sedlin (the mammalian ortholog of yeast Trs20p) revealed an unexpected similarity to the structures of the N-terminal regulatory domain of two SNARE proteins, Ykt6p and Sec22b, suggesting that sedlin may play a regulatory role in the pairing of SNAREs in the early secretory pathway (Jang et al., 2002). Recently, we and others have shown that Bet3p plays a critical role in anchoring TRAPP specifically to the Golgi (Kim et al., 2005b; Turnbull et al., 2005), a process that depends on both a flat, positively charged surface and a hydrophobic channel (Kim et al., 2005b). Subsequently, we determined the structure of bet3 in complex with trs33. The tertiary structure of trs33 is closely similar to that of bet3 but lacks the hydrophobic channel seen in bet3 (Kim et al., 2005a; Turnbull et al., 2005).

Clarification of TRAPP architecture will be a crucial step toward the elucidation of the virtually unknown molecular mechanism of the tethering process mediated by these complexes. Here, we report the molecular interactions between all six subunits constituting vertebrate and yeast TRAPP I. This led to the identification of the bet3-trs33-bet5-trs23 heterotetramer and the bet3-trs31-sedlin heterotrimer as the two stable subcomplexes of mammalian TRAPP I, and the crystal structures of these subcomplexes were solved. In contrast, the yeast orthologs of these proteins form a functional and stable six-subunit complex. Single-particle electron microscopy revealed that the yeast TRAPP I complex has an elongated, bilobal overall shape, which nicely accommodates the crystal structures of the mammalian subcomplexes. Together with the identification of the minimal unit required for Ypt1p guanine nucleotide exchange factor (GEF) activity, this detailed architectural analysis of the complete TRAPP I tethering factor allows us to present a model by which this complex imparts specificity in ER-to-Golgi traffic.

RESULTS

Formation of Mammalian TRAPP I Subcomplexes

In order to examine the network of interactions between the TRAPP I subunits, we utilized an *in vitro* system using purified individual subunits. We could purify a total of five subunits (bet3, bet5, trs23, trs33, and sedlin) to homogeneity but were able to detect only two binary interactions: the formation of the complexes between bet3 and trs33 and between bet5 and trs23. Because mammalian trs31 could not be expressed in *E. coli*, we resorted to the trs31 ortholog from zebrafish (hereafter referred to as trs31), which displays very high sequence identity (80%) with its mammalian counterparts. Coexpression of trs31 with bet3 resulted in the purification of a heterodimer between the two proteins. Because we suspected that some TRAPP subunits may interact with two subunits simultaneously, the bet3-trs33 and bet3-trs31 heterodimers were incorporated into the *in vitro* binding assay. As demonstrated by a glutathione S-transferase (GST) pull-down assay (Figure 1A), sedlin interacted strongly with only the bet3-trs31 heterodimer. In contrast, a GST-bet5 fusion protein interacted with the bet3-trs33 heterodimer and trs23, but not with any of the other proteins. Quantitation of the bands on the gel indicates a 1:1:1 stoichiometry for the bet3-trs31-sedlin complex and a 1:1:2 stoichiometry for the bet3-trs33-bet5 complex, consistent with their molecular sizes on a size-exclusion column (51 kDa and 71 kDa, respectively; Figure 1B). Incubation of trs23 with the bet3-trs33-bet5 complex resulted in the production of a four-subunit complex. Gel filtration followed by electrophoretic analysis of the mixture indicated that one copy of bet5 in the three-subunit complex was slowly replaced by trs23 (Figure 1B). However, when bet3, trs33, bet5, and trs23 were coexpressed in *E. coli*, they readily formed a heterotetramer (86 kDa) with a 1:1:1:1 stoichiometry as estimated by gel filtration (data not shown) and

confirmed by the structure determination as described below. The tetrameric complex did not interact with the bet3-trs31-sedlin complex in the analyses by gel filtration and GST pull-down. These observations strongly suggest that vertebrate TRAPP I is composed of the tetrameric and trimeric subcomplexes and that an as yet unidentified vertebrate subunit may link these complexes.

Expression of rTRAPP I

To investigate whether the corresponding subcomplexes can be produced with the yeast counterparts, we carried out coexpression experiments in *E. coli* rather than a similar *in vitro* binding assay because all hexahistidine-tagged yeast orthologs were insoluble when expressed individually. The Trs85p subunit was omitted from these studies since it is nonessential to the function of TRAPP I. Of the remaining subunits, only Trs33p is nonessential. This subunit was included in these studies because (1) it interacts with Bet3p (Kim et al., 2005a) and (2) deletion of two nonessential TRAPP subunits can be lethal (Tong et al., 2001). Indeed, upon coexpression of TRAPP I subunits, stable Bet3p-Trs33p-Bet5p and Bet3p-Trs31p-Trs20p complexes were produced (Figure 1C). Quantitation of the bands on the SDS gels indicated a 1:1:1 stoichiometry for both subcomplexes. While this stoichiometry was supported by size-exclusion chromatography for the Trs20p-containing subcomplex (~75 kDa; Figure 1C), both size-exclusion chromatography (Figure 1C) and dynamic light scattering (data not shown) indicated that the Bet5p-containing complex was likely to be a dimer of trimers (~160 kDa). When each trimeric complex was coexpressed with Trs23p, stable tetrameric complexes of Bet3p-Trs33p-Bet5p-Trs23p and Bet3p-Trs31p-Trs20p-Trs23p were formed (Figure 1D), and both exhibited a 1:1:1:1 stoichiometry. Reasoning that Trs23p might serve to link the two heterotrimeric complexes together, we coexpressed all six yeast TRAPP I subunits using three dual-expression vectors. Strikingly, when all six yeast proteins were coexpressed, a stable complex was formed. Quantitation of the bands on the SDS gel indicated a stoichiometry of 2:1:1:1:1:1 with respect to Bet3p:Trs33p:Trs31p:Trs23p:Trs20p:Bet5p, supported by the apparent size of ~170 kDa on a size-exclusion column (Figure 2A). The fact that Bet3p is present at twice the level of the other subunits is consistent with its interaction with both Trs31p and Trs33p and is consistent with an earlier study that showed the presence of at least two copies of Bet3p in TRAPP I (Sacher et al., 2000). These results indicate that the six coexpressed TRAPP I subunits self-assemble into a recombinant TRAPP I complex herein referred to as rTRAPP I. The complex was not formed when the Trs23p subunit was omitted from the coexpression vector (data not shown), strongly suggesting that Trs23p links the two heterotrimeric subcomplexes together to form the rTRAPP I complex.

To verify that the six subunits are components of the same complex, we examined the peak fraction from the size-exclusion column by several methods. First, static

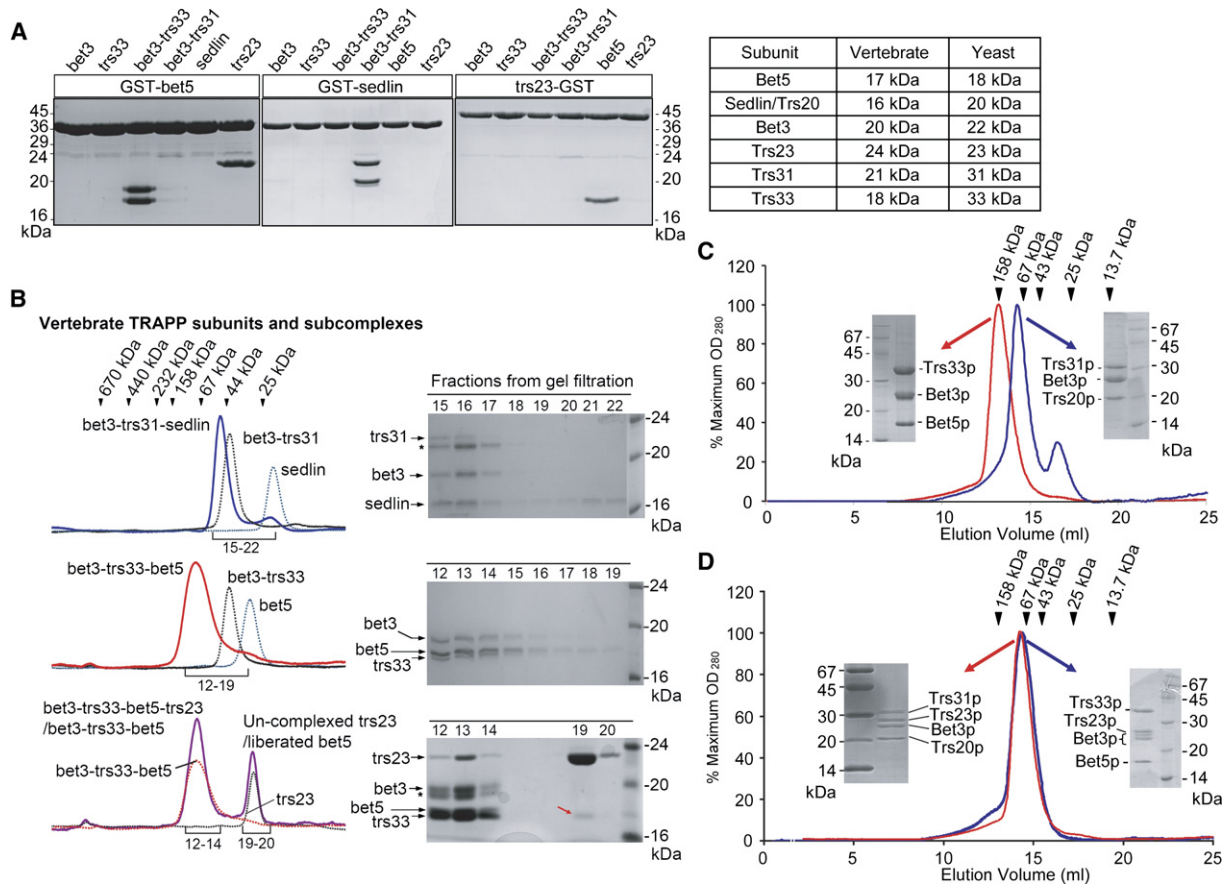


Figure 1. Interactions between Mammalian and Yeast TRAPP Subunits

(A) The indicated TRAPP components or heterocomplexes were incubated with GST-tagged bet5, sedlin, or trs23, and resin-bound proteins were detected by SDS-PAGE. The apparent sizes of the vertebrate and yeast subunits used in these studies are shown in the table to the right.

(B) The mixture of sedlin and bet3-trs31, bet5 and bet3-trs33, or trs23 and bet3-trs33-bet5 was analyzed by gel filtration. Each of the relevant fractions is shown in the right panels and corresponds to the solid line traces to the left. Bands marked by asterisks are truncated forms of trs31 and bet3 as determined by mass spectrometry. The red arrow in the lower panel indicates the liberated bet5 from the bet3-trs33-bet5 complex. The apparent substoichiometric amount of trs23 on the gel indicates that the peak from the column is a mixture of bet3-trs33-bet5 and bet3-trs33-bet5-trs23. The apparent discrepancy in the amount of bet5 displaced by trs23 (lower panel, fraction 19) is most likely due to the instability and/or degradation of the monomeric bet5 protein.

(C) The yeast proteins Bet3p, Trs31p, and Trs20p or Bet3p, Trs33p, and Bet5p were coexpressed in *E. coli* and analyzed by gel filtration. A fraction from each peak is shown. The elution positions of standard size markers are indicated by arrowheads.

(D) The yeast proteins Bet3p, Trs31p, and Trs20p or Bet3p, Trs33p, Bet5p, and Trs23p were coexpressed, purified, and analyzed as in (C). Stoichiometries reported in the text are not definitive due to the possibility of nonequivalent dye binding to the proteins and protein degradation but are supported by the crystal structures and the subsequent EM analysis.

light scattering suggests a monodispersed sample (data not shown). Second, the proteins migrate as a single band on a nondenaturing polyacrylamide gel (data not shown), suggesting that only one species is present in the fraction. Finally, the subunits bind to and elute from an ion-exchange column as a single unit (data not shown).

Functional Analysis of rTRAPP I

In order to validate any further structural analyses, it was necessary to show that rTRAPP I behaves similarly to TRAPP I purified directly from yeast (herein referred to as TRAPP I). It was previously shown that TRAPP I acts as a GEF for the GTPase Ypt1p (Jones et al., 2000;

Wang et al., 2000). We therefore tested whether rTRAPP I could exchange nucleotide on this GTPase. To assay for GEF activity, ³H-GDP was bound to Ypt1p and the ability of rTRAPP I and various subcomplexes to release the bound, radiolabeled nucleotide was assayed. As a control, we also assayed Dss4p, a protein with a broad spectrum of GEF activity. As shown in Figure 2B, compared to Dss4p, rTRAPP I displayed potent Ypt1p GEF activity. The release of nucleotide was essentially complete within 5 min of addition of the GTPase. These results indicate that rTRAPP I is an assembled and active form of TRAPP I.

To narrow down the active region of rTRAPP I, we assayed the ability of subcomplexes to release nucleotide

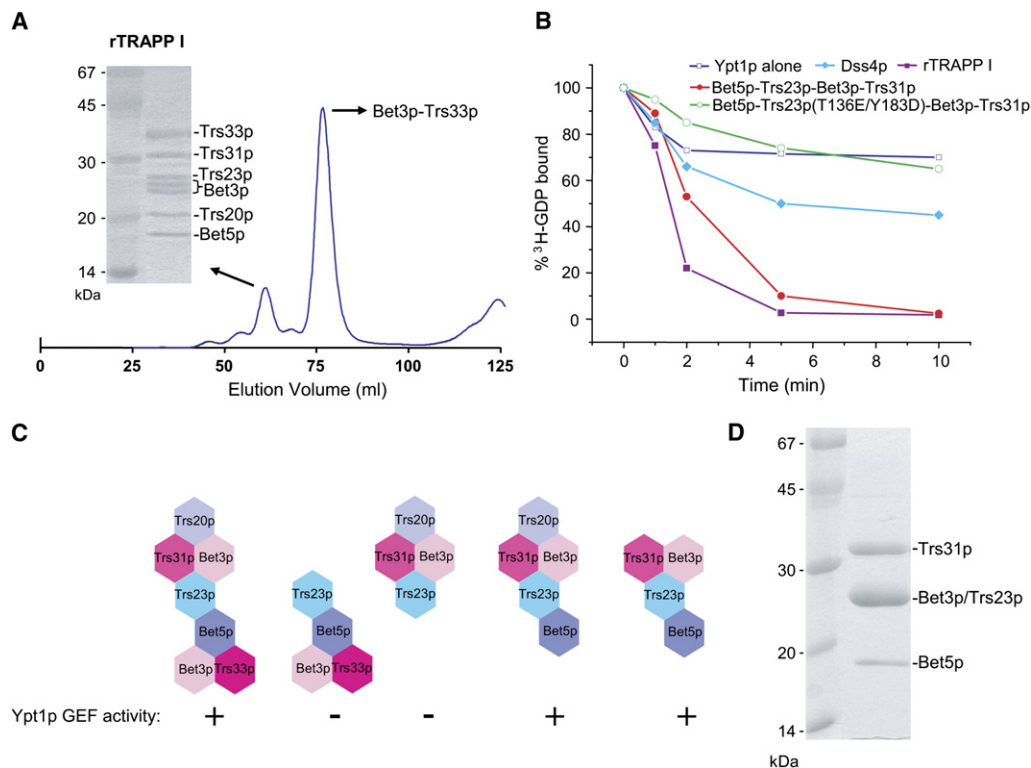


Figure 2. Functional Analysis of rTRAPP I

(A) All six TRAPP I subunits were coexpressed and fractionated by gel filtration. The peak at ~170 kDa (leftmost peak) was analyzed by SDS-PAGE (inset) and represents the assembled rTRAPP I complex. A Bet3p doublet, seen here, is often seen when TRAPP I is purified from yeast (see [Sacher et al., 1998, 2001](#)).

(B) Nucleotide exchange activity was assayed for rTRAPP I (purple line), Bet5p-Trs23p-Bet3p-Trs31p (red line), Bet5p-Trs23p(T136E/Y183D)-Bet3p-Trs31p (green line), Dss4p (cyan line), or Ypt1p alone (blue line).

(C) A graphical representation of the results of the TRAPP I subcomplexes assayed for GEF activity.

(D) The TRAPP I subunits Trs23p, Bet5p, Bet3p, and Trs31p were coexpressed in *E. coli*, and the heterotetrameric complex was purified. The comigration of Bet3p and Trs23p was confirmed by N-terminal sequence analysis.

from Ypt1p. Neither the Bet3p-Trs33p-Bet5p-Trs23p nor the Bet3p-Trs31p-Trs20p-Trs23p heterotetrameric subcomplexes could support nucleotide release (Figure 2C). This strongly suggested that subunits in both of these subcomplexes are needed for this function. Indeed, the addition of Bet5p to the Bet3p-Trs31p-Trs20p-Trs23p subcomplex resulted in GEF activity (Figure 2C). The most reasonable assumption is that the subunits closest to Trs23p, the linker between the heterotrimeric subcomplexes, are required for this activity. Therefore, we needed to determine the arrangement of the subunits in the Bet3p-Trs31p-Trs20p-Trs23p subcomplex. Coexpression of Trs23p-Bet5p-Trs20p did not lead to the identification of such a subcomplex. However, we could coexpress and purify the heterotetramer Bet5p-Trs23p-Bet3p-Trs31p (Figure 2D), suggesting that Trs23p links Bet5p to the Bet3p-Trs31p dimer with Trs20p bound elsewhere to the dimer. When we assayed this heterotetramer for GEF activity, we found that it was nearly as active as rTRAPP I in releasing nucleotide from Ypt1p (Figure 2B). The fact that rTRAPP I was slightly more active than Bet5p-Trs23p-

Bet3p-Trs31p could reflect a slight difference in the structures of these subunits when found within the fully assembled complex. These results suggest that the minimal unit needed for GEF activity is Bet5p-Trs23p-Bet3p-Trs31p. Previous studies resulted in conflicting data as to whether TRAPP could also act as a GEF for the GTPases Ypt31p and Ypt32p, which function later in the secretory pathway than Ypt1p (Jones et al., 2000; Wang et al., 2000). We found that rTRAPP I was incapable of releasing nucleotide from either of these two GTPases (data not shown), suggesting that TRAPP I is a GEF for only Ypt1p.

Structure and Intermolecular Interactions of the bet3-trs31-sedlin Subcomplex

The structure of the bet3-trs31-sedlin subcomplex was determined at 2.1 Å resolution. The bet3 and trs31 monomeric structures are similar to each other except for the presence of an additional C-terminal α helix in trs31 (Figure 3; see also Figure S1 in the Supplemental Data available with this article online). However, a clear difference is that while bet3 has a prominent central channel that

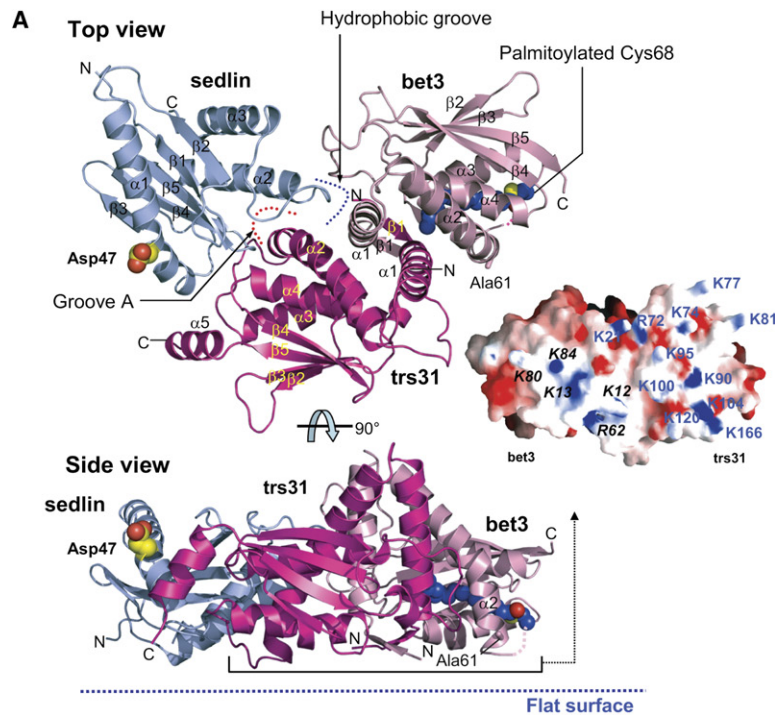
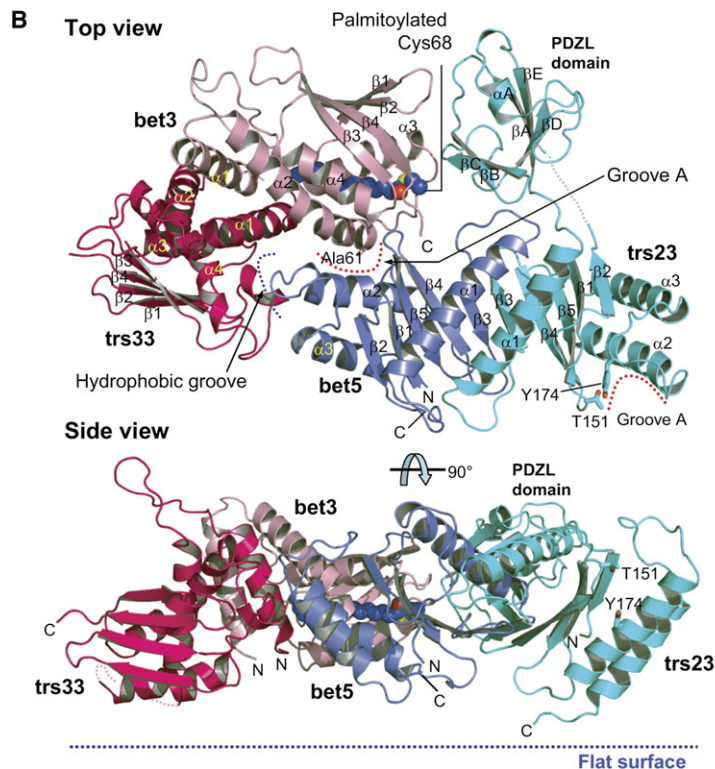


Figure 3. Structures of the bet3-trs31-Sedlin and bet3-trs33-bet5-trs23 Sub-complexes

(A) Ribbon drawings of the bet3-trs31-sedlin subcomplex. Two perpendicular views of the structure are shown. The secondary structures are numbered in order of their appearance in the sequence. Asp47 of sedlin (a SEDL-causing point mutation) and palmitoylated Cys68 of bet3 are shown in CPK models. Dashed lines indicate the disordered regions in the crystal structure. A surface representation of the flat surface of the bet3-trs31 portion is shown. The positive and negative charges are in blue and red, respectively. The basic residues of bet3 and trs31 responsible for the positive charges are labeled with black italic and blue bold letters, respectively.

(B) Ribbon drawings of the bet3-trs33-bet5-trs23 subcomplex. The molecular complex is presented similarly to that in (A), with the bet3-trs33 unit in an orientation similar to bet3-trs31. The residues probed by mutational analysis are shown in sticks and labeled in (A) and (B). The flat surfaces of the subcomplexes are presumed to face the Golgi membrane.



can fully accommodate a myristoyl or palmitoyl group covalently attached to a cysteine residue (Kim et al., 2005a, 2005b; Turnbull et al., 2005), trs31 does not. Although trs31 exhibits 11% and 14% sequence identity with bet3 and trs33, respectively, the structure of trs31 is more sim-

ilar to that of bet3 than that of trs33 (Figure S1). The bet3-trs31 heterodimer interacts with sedlin in a side-by-side manner to form a flat subcomplex in which sedlin interacts predominantly with trs31 mainly by using two shallow grooves. One groove (referred to as groove A) is formed

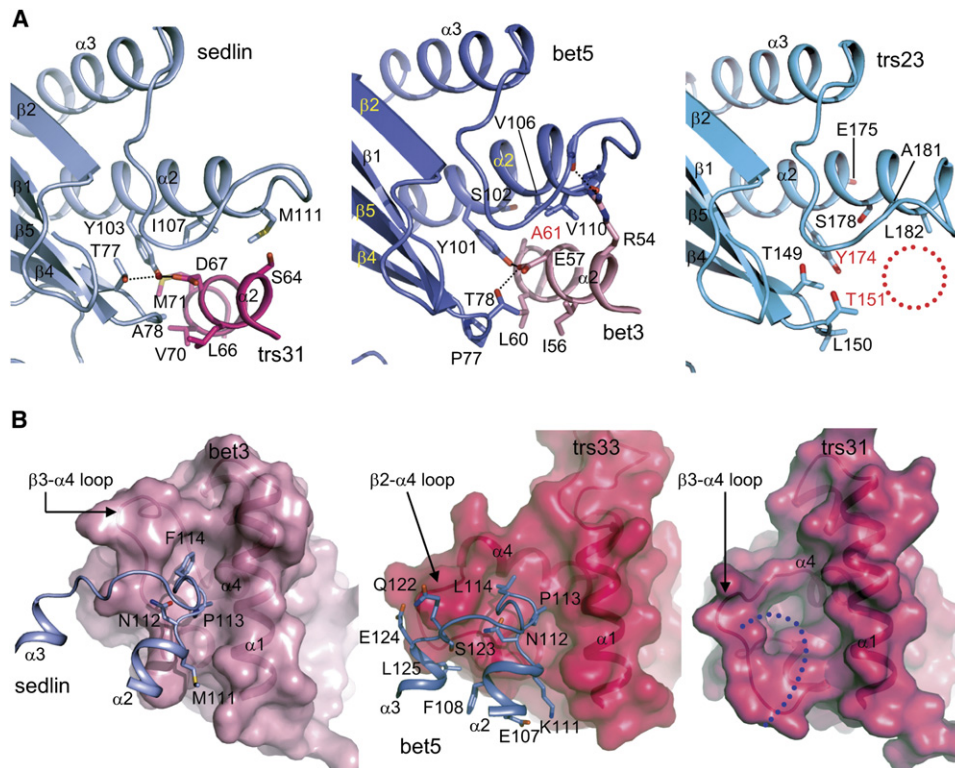


Figure 4. Focused Structural Views

(A) Detailed views of groove A of the sedlin family subunits. Groove A of sedlin and bet5 is occupied by $\alpha 2$ of trs31 and bet3, respectively, while that of trs23 in the heterotetramer is unoccupied (dotted red circle). The conserved residues at groove A and/or interacting with the groove are shown. The residues probed by mutational analysis are labeled with red letters.

(B) Detailed views of the hydrophobic groove of the bet3 family subunits. The groove of bet3 and trs33 is occupied by a segment of sedlin and bet5, respectively, while that of trs31 is unoccupied (highlighted with a dashed curve). The conserved residues interacting with the groove are shown as sticks.

by a part of $\alpha 2$ and loop $\beta 4$ - $\beta 5$ of sedlin and accepts $\alpha 2$ of trs31 (Figure 3A and Figure 4A). The other groove is formed by the C-terminal part of $\alpha 1$, loops $\alpha 1$ - $\beta 3$, and $\beta 4$ - $\beta 5$ of sedlin. It accepts the $\alpha 2$ - $\alpha 3$ loop of trs31 (Figure 3A). These interactions bury a solvent-accessible surface area of 742 Å² of trs31. At the bet3-sedlin interface, a conserved segment in loop $\alpha 2$ - $\alpha 3$ of sedlin, which was proposed as a putative protein-binding motif (Jang et al., 2002), is snugly docked to the hydrophobic groove of bet3 formed by helix $\alpha 1$ and loop $\beta 3$ - $\alpha 4$ (Figure 4B), burying a solvent-accessible surface area of 385 Å². By interacting with the C-terminal helix of trs31, sedlin undergoes a conformational change in $\alpha 1$: a 6.5-turn helix in the complex, as opposed to a 4-turn helix in the isolated protein (Jang et al., 2002). As a result, while free sedlin is structurally similar to the N-terminal regulatory domain of the SNARE proteins Ykt6p and Sec22b (Jang et al., 2002), sedlin in the heterotrimeric subcomplex more closely resembles these SNAREs. The bet3-trs31 portion in the trimeric subcomplex has an unusually flat, wide, positively charged surface that is comprised of residues from both subunits (Figure 3A). The lysine and arginine residues in trs31 on this surface are nearly invariant in the metazoan

orthologs (Figure S2). Previously, a charge-inversion mutation of two conserved lysine residues (Lys24 and Lys96) on this surface of yeast Bet3p was shown to result in a Bet3p mutant protein that remained predominantly in the cytosol (Kim et al., 2005b), and overexpression of TRS33, which also has a flat, positively charged surface, drove this mutant Bet3p to Golgi membranes (Kim et al., 2005a). Given these observations, the flat surface of the bet3-trs31 complex is presumed to be the membrane-proximal surface.

Structure and Intermolecular Interactions of the bet3-trs33-bet5-trs23 Subcomplex

The structure of the bet3-trs33-bet5-trs23 subcomplex was determined at 2.4 Å resolution. The four subunits are arranged to form an unusually flat molecular complex through the side-by-side interactions between bet3-trs33 and bet5 and between bet5 and trs23 (Figure 3B). The structure of the bet3-trs33 portion in this subcomplex is virtually the same as that of the bet3-trs33 heterodimer reported earlier (Kim et al., 2005a) and is similar to the bet3-trs31 unit in the trimeric subcomplex.

The bet5 subunit (145 residues) is composed of 5 β strands and 3 α helices that are arranged to form an α/β fold, with the single β sheet sandwiched by the N-terminal α helix at one side and the C-terminal antiparallel α helices at the other side (Figure 3B). The folding topology and the number of secondary structural elements of bet5 are identical to those of sedlin (140 residues), which exhibits 10% sequence identity with bet5. The structure of bet5 is most similar to that of isolated sedlin (Jang et al., 2002) in the Protein Data Bank (ID code 1H3Q) and even more similar to that of sedlin in the trimeric subcomplex (Figure S3). Although bet5 and sedlin are structurally similar, as are bet3-trs33 and bet3-trs31, bet5 binds to a surface of bet3-trs33 opposite to the interface of bet3-trs31 for binding sedlin in the trimeric subcomplex. As a consequence, the position of bet5 relative to bet3-trs33 in the tetrameric subcomplex is completely different from the position of sedlin relative to bet3-trs31 in the trimeric subcomplex (Figures 3A and 3B). Like groove A of sedlin, the corresponding groove of bet5 is shallow and accepts $\alpha 2$ of bet3 (Figure 3B and Figure 4A). In addition, parts of $\alpha 2$, $\alpha 3$, and loop $\alpha 2$ - $\alpha 3$ of bet5 lean tightly against the hydrophobic groove of trs33 formed by the helices $\alpha 1$ and $\alpha 4$ and loop $\beta 2$ - $\alpha 4$ (Figure 3B and Figure 4B).

The trs23 subunit (219 residues) is composed of two domains (Figure 3B). One is a sedlin-like domain (140 residues), which is very similar to bet5 in the three-dimensional structure (Figure 3B and Figure S3A). While an alignment of the whole sequence of trs23 and bet5 showed only limited homology between the two proteins, a structure-based sequence alignment of the sedlin-like domain of trs23 and bet5 revealed that the two domains are similar not only in the length of the polypeptides but also at the primary sequence level (22% identity) (Figure S3B). The sedlin-like domain of trs23 and bet5 bind to each other primarily through the intermolecular packing of the $\alpha 1$ helices cradled by the gently curved intermolecular β sheet formed by the juxtaposition of the β sheets of the two subunits (Figure 3B). With the very high structural similarity and the extensive binding interface (1785 Å²) between the two proteins, the bet5-trs23 heterodimeric interaction looks like a stable homodimeric interaction related by a 2-fold symmetry.

The other domain of trs23 (residues 23–101) is present in the middle of the polypeptide and is connected to the sedlin-like domain by two flexible loop segments (Figure 3B) whose electron densities are weak or missing. This domain exhibits barely detectable sequence homology to several PDZ domains, with the highest similarity to the sixth PDZ domain of InaD-like protein (INADL). However, the sequence similarity is limited to the C-terminal 40 residues (Figure S4A), as observed by others (Ethell et al., 2000). Furthermore, the domain in trs23 does not have the Gly-Leu-Gly-Phe signature sequence of a classical PDZ domain. We therefore refer to the second domain in trs23 as the PDZ-like (PDZL) domain. This domain of trs23 interacts with bet3, but with poor shape complementarity at the interface involving two hydrogen bonds

and a few van der Waals interactions. Since the interactions are weak and the peptide linkers between the two domains of trs23 are long and flexible, the PDZL domain is likely to have the freedom to move relative to the rest of the subcomplex.

Identification of Residues Critical for TRAPP I Function

Through mutational analysis, we identified Ala61 of bet3 (Ala73 in yeast Bet3p) as a critical residue in the function of TRAPP I. Mutation of this residue in the yeast protein to either leucine or aspartic acid resulted in an extremely sick strain or lethality, respectively (Figure 5A). Coexpression of these Bet3p mutants in *E. coli* with Trs33p and Bet5p or with Trs31p, Trs23p, and Bet5p indicated that the Bet3p-Bet5p interaction and the Bet3p-Trs23p interaction were disrupted (Figure 5B, lanes 1–6). While Ala61 of bet3 is exposed in the trimeric subcomplex, this residue in the tetrameric subcomplex is completely buried by bet5 (Figures 3A and 3B). This indicates that the structurally similar Bet5p and Trs23p proteins interact with Bet3p via common Bet3p residues and further indicates that an assembled complex is vital for the vegetative growth of yeast. Since two copies of Bet3p are present in the complex, these interactions are not mutually exclusive.

We next examined the mutational effect of Thr136 and Tyr183 in Trs23p, which correspond to Thr151 and Tyr174 in trs23 located at groove A of this subunit (Figure 3B and Figure 4A). A Trs23(T136E/Y183D) double mutant was also found to be lethal in yeast (Figure 5A). While this mutated subunit was incorporated into the Bet5p-Trs23p-Bet3p-Trs31p complex (Figure 5B, lane 7), the minimal unit required for GEF activity, this subcomplex failed to exchange nucleotide on Ypt1p (Figure 2B). Presumably, groove A (and perhaps surrounding regions) is responsible for the TRAPP I-associated GEF activity.

The PDZL Domain of trs23 Appears as a Metazoan-Specific Protein-Binding Module

PDZ domains bind peptide segments, usually a C-terminal four-residue segment (Nourry et al., 2003). A database search revealed that the second PDZ domain of syntenin in complex with an Asn-Glu-Phe-Tyr-Ala peptide is structurally most similar to the PDZL domain of trs23. In the syntenin PDZ domain, the Gly-Leu-Gly-Phe signature sequence lines a prominent cavity of this domain and forms a cradle of backbone -NH groups that charge balance the C-terminal carboxylate group of the bound peptide, which conforms to the classical interactions observed for the 20 other PDZ-peptide complex structures in the structural database. The cavity of syntenin also accepts the methyl group of the last residue (alanine) of the peptide. The corresponding cavity is present in the PDZL domain of trs23 (Figure S4B). However, this cavity is unlikely to interact with the -COO⁻ group because the Pro35-Leu36-Asp37-Leu38 sequence instead of the Gly-Leu-Gly-Phe signature of the classical PDZ domains places the carbonyl oxygens

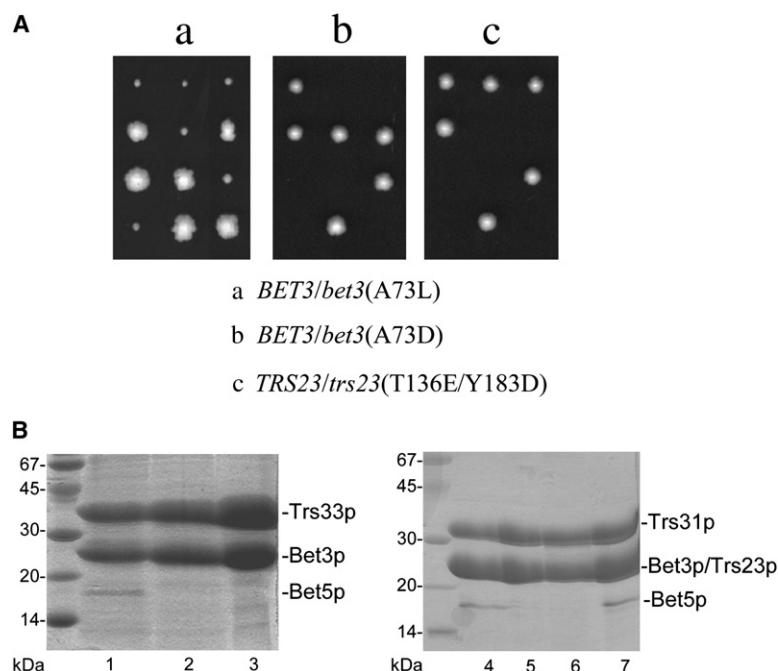


Figure 5. Effects of Mutations in the Bet3p and Trs23p Subunits on Protein Interactions within TRAPP I

(Aa–Ac) The indicated diploids were sporulated and dissected. Three representative spores are shown for each. Plates were incubated at 25°C for either 3 days (Ab and Ac) or 6 days (Aa). Note that the larger, less rounded-shaped colonies in (Aa) are *BET3*, while the much smaller colonies, visible only after 5–6 days of growth, are *bet3(A73L)*.

(B) The following coexpressions in *E. coli* were performed: Trs33p and Bet5p with either Bet3p (lane 1), Bet3p(A73D) (lane 2), or Bet3p(A73L) (lane 3); Trs23p, Bet5p, and Trs31p with either Bet3p (lane 4), Bet3p(A73D) (lane 5), or Bet3p(A73L) (lane 6); and Bet3p, Bet5p, and Trs31p with Trs23p(T136E/Y183D) (lane 7). Equal amounts of protein from each expression were loaded on the gel following metal-affinity chromatography. The large excess of Bet3p and Trs33p in lanes 1–3 and Bet3p and Trs31p in lanes 4–7 represents the Bet3p–Trs33p and Bet3p–Trs31p heterodimers, respectively. The presence of Trs23p in lanes 4 and 7 was verified by N-terminal amino acid sequence analysis.

of Leu36 and Leu38 into the cavity, which would cause electrostatic repulsion against the $-\text{COO}^-$ group, and it does not have an alternative feature to stabilize the $-\text{COO}^-$ group. Furthermore, the cavity of the PDZL domain is shallower than that of the syntenin PDZ domain. Since the cavity is predominantly hydrophobic, it is unlikely to bind a polar head group of the phospholipid bilayer. We suggest that the PDZL domain of trs23 is a protein-binding module, interacting with an internal segment of a protein. While the sequence identity of five TRAPP subunits (*bet3*, *bet5*, *trs31*, *trs33*, and *sedlin*) is unusually high (27%–54%) between yeast and human, yeast Trs23p and human trs23 exhibit only 22% sequence identity. However, with the omission of the PDZL domain sequence based on the structure, human trs23 exhibits 45% sequence identity with yeast and fungal Trs23p (Figure S5). The PDZL domain sequence is absent in the Trs23p proteins of single-cell eukaryotes, and the domain was thus newly added during the evolution of metazoans.

Electron Microscopy and Single-Particle Analysis of rTRAPP I

As the next step in the structural characterization of TRAPP I, we examined the morphology of rTRAPP I by single-particle electron microscopy (EM). Images of negatively stained samples were recorded, and the complex was shown to be monodisperse and homogeneous in size and overall shape (Figure 6A), suggesting that the particles adsorbed to the carbon support film in a preferred orientation. We therefore had to record image pairs at tilt angles of 60° and 0° to obtain the different views needed to calculate a three-dimensional (3D) density map of the rTRAPP I complex with the random conical tilt approach

(Radermacher et al., 1987). We interactively selected about 9500 particle pairs and classified the particle images of the untilted specimen into 100 classes. Representative class averages are shown in Figure 6B. The differences seen between individual class averages may represent a different level of stain embedding, rotation of the particle about its long axis, or slight conformational changes. We then merged the images from three classes that produced very similar averages (about 1900 particle pairs) and calculated a 3D reconstruction of the complex (Figure 6D). The resulting density map had a resolution of about 30 Å as judged by Fourier shell correlation. The elongated complex, with approximate dimensions of 180 Å × 65 Å × 50 Å (length × width × height), has a bilobal organization. In the top view (Figure 6D, top panel) the left lobe has a round shape, whereas the right lobe has a triangular shape, which was already observed in most of the class averages (Figure 6B). The two lobes each contain an additional smaller density, which come together in the middle of the complex and form the connection between the two lobes.

Docking of Crystal Structures into the EM Density Map of rTRAPP I

The two lobes of the single-particle reconstruction have very similar shapes. It was therefore not immediately evident how the crystal structures of the mammalian subcomplexes *bet3*–*trs31*–*sedlin* (Figure 3A) and *bet3*–*trs33*–*bet5*–*trs23* (Figure 3B) should be fit into the density map of the yeast complex. To resolve this ambiguity, we labeled the rTRAPP I complex with Fab fragments against Trs33p. The class averages (Figure 6C) showed that the Fab fragments bound specifically to the rounder lobe of

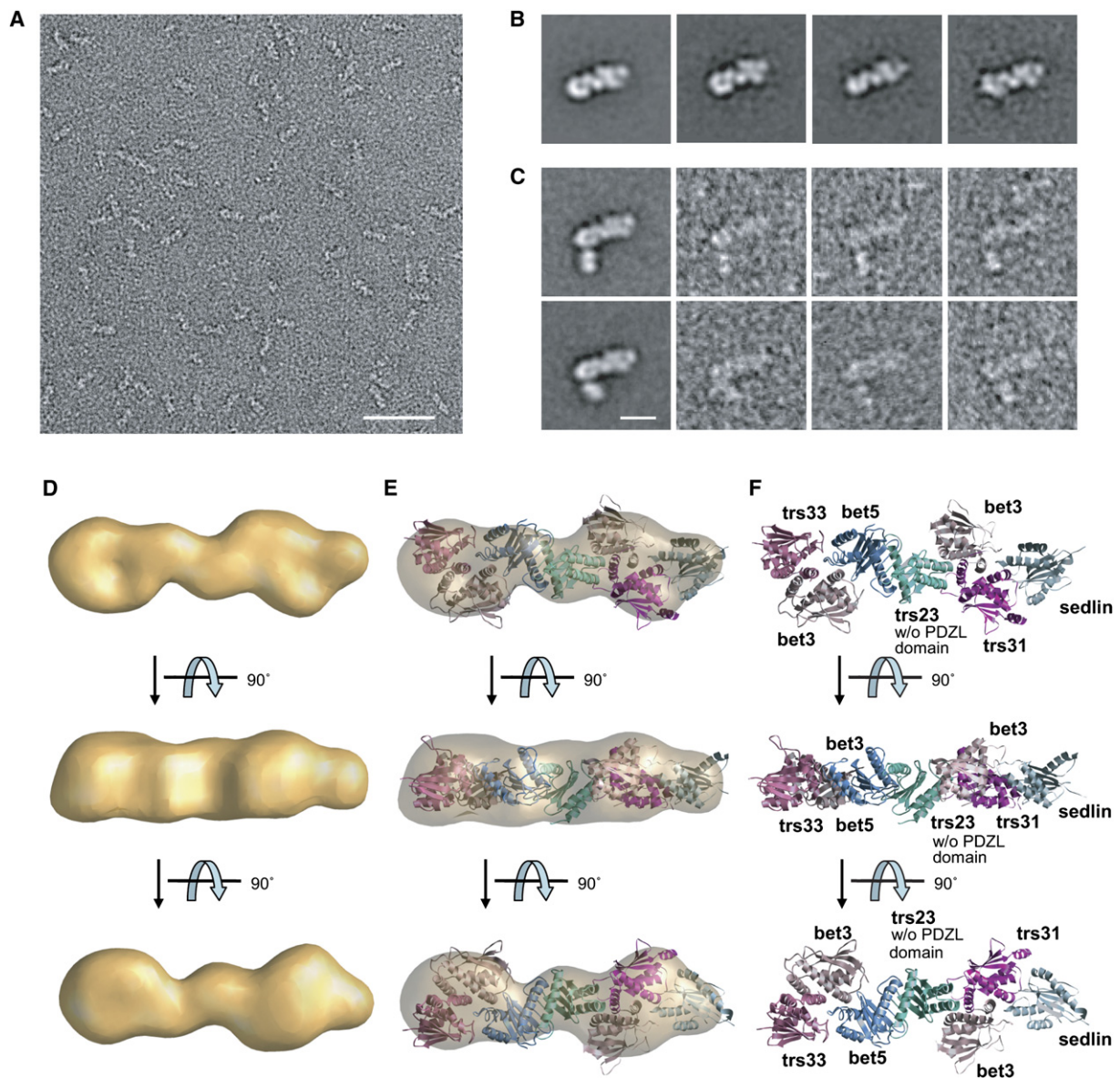


Figure 6. Single-Particle Electron Microscopy of Yeast rTRAPP I Complex and Docking of the Crystal Structures

(A) Typical electron micrograph area of rTRAPP I negatively stained with uranyl formate. Scale bar = 50 nm.

(B) Representative class averages, each containing between 200 and 500 particles, after alignment and classification of about 9500 particle images. Scale bar = 10 nm.

(C) Labeling with Fab fragments against Trs33p. Left panels show two class averages (top, 84 particles; bottom, 122 particles) after alignment and classification of 914 particle images. Panels to the right show representative raw particle images of the corresponding classes. Scale bars = 10 nm.

(D) Views of the 3D density map of the yeast rTRAPP I complex obtained with the random conical tilt approach.

(E and F) The crystal structures of the mammalian subunits were fit into the volume of the yeast complex. The PDZL domain of trs23 is lacking in yeast Trs23p and was therefore removed from the crystal structure. If the PDZL domain is included for the fitting, it protrudes from the density map close to the middle of the complex (Figure S6).

the rTRAPP I complex (left side in Figure 6D). The round lobe must therefore represent the tetrameric complex composed of bet3-trs33-bet5-trs23, and the more triangular lobe the trimeric subcomplex composed of bet3-trs31-sedlin. This assignment was used to visually fit the

crystal structures of the two subcomplexes into their respective densities (Figure 6E). The PDZL domain of mammalian trs23 is lacking in its yeast ortholog Trs23p and was therefore removed from the crystal structure for fitting into the EM map (Figure 6E). If included, the PDZL domain

protrudes from the density map close to the middle of the complex (Figure S6). The docking of the crystal structures into the density map revealed that the two subcomplexes interact with each other through contacts between bet3 and trs31 of the trimeric subcomplex and trs23 of the tetrameric subcomplex (Figure 6F). This orientation of the subcomplexes in TRAPP I is consistent with the ability to express and purify a Bet5p-Trs23p-Bet3p-Trs31p heterotetramer (Figure 2D) and the data showing that this subcomplex represents the minimal unit for Ypt1p GEF activity (Figure 2B).

Our density map of the elongated complex appears to be rather flat, especially on the side expected to be in contact with the membrane (Figure 6D, side view). Because of the good fit of the crystal structures of the subcomplexes into the EM density map, the flatness appears to be a real feature of the complex and does not seem to be due to specimen flattening, an artifact often encountered with negatively stained specimens (Cheng et al., 2006). To compare the mammalian and the yeast TRAPP I complexes, we calculated homology models for the yeast proteins based on the crystal structures of the mammalian proteins and fit those into the density map of the yeast complex (see Figure S6). The homology models produced a fit into the density map similar to the crystal structures of the mammalian subcomplexes, further corroborating the accuracy of our single-particle reconstruction.

DISCUSSION

The ability to produce large amounts of an assembled, functional TRAPP I complex allows for the examination of its biochemical properties, which was previously hampered by the low amounts of this complex in cells. Structural information is now available for six different vertebrate TRAPP subunits that can be divided into two families: the bet3 family composed of bet3, trs31, and trs33 and the sedlin family composed of sedlin, bet5, and trs23. The functional roles of the subunits would include (1) Golgi targeting/localization, (2) COPII vesicle capture, (3) GEF activity, and (4) regulation of the v- and t-SNARE pairing. One apparent function of bet3-trs33 and bet3-trs31 lies in the Golgi localization of the other subunits by forming tight subcomplexes of bet3-trs31-sedlin and bet3-trs33-bet5-trs23. Since the yeast six-subunit complex contains two copies of Bet3p, this complex may not depend on Trs31p and Trs33p for membrane targeting. In this regard, it is noteworthy that many of the basic residues on the flat surface of trs31 that are nearly invariant in the metazoan orthologs are not conserved in yeast Trs31p (Figure S2), and charge-inversion mutations of conserved basic residues on the flat surface of Trs33p did not affect its targeting to the membrane (Kim et al., 2005a). Consistent with a previous study suggesting that individual TRAPP subunits do not possess Ypt1p GEF activity (Wang et al., 2000), we have shown that the minimal region of the TRAPP I complex required for this activity is composed of the subcomplex Bet5p-Trs23p-Bet3p-

Trs31p. Interestingly, the strongest suppressors of the yeast *bet3-1*, *bet3-3*, and *bet3-4* mutations are the *BET5* and *TRS23* genes (Jiang et al., 1998; Kim et al., 2005b; Sacher et al., 1998; M.S., unpublished data), supporting a role for all three of these gene products in a common process. Given the involvement of groove A of Trs23p in GEF activity, it is likely that other highly conserved residues nearby are also involved in this function (Figure 7A), and preliminary data support this notion (M.S., unpublished data). Finally, we suggest that a putative function of the sedlin/Trs20p subunit lies in the regulation of SNARE pairing through interaction with the regulatory domain or SNARE domain of a SNARE protein (see below).

A Model for TRAPP I-Mediated Vesicle Tethering

The complete architecture of the TRAPP I complex allows us to propose a model for vesicle tethering at the Golgi (Figure 7B). Although the mechanism of vesicle tethering is unclear, it has been suggested that long, extended coiled-coil proteins such as p115, GM130/golgin-95, and the yeast Uso1p act by projecting lengthwise from the membranes to be fused (Lowe, 2000; Pfeffer, 1996; Waters and Hughson, 2000; Whyte and Munro, 2002). We now know that if TRAPP I were to act by a similar mechanism, this would still leave ~180 Å to be bridged for vesicle fusion. Furthermore, interaction of v- and t-SNAREs, to produce the fusogenic SNAREpin structure (Weber et al., 1998), occurs over a length of 130–140 Å (Hanson et al., 1997). Therefore, several models suggest that the extended vesicle tether needs to be removed from the site of fusion to allow the membranes to come into close enough proximity for SNAREpin formation to occur. We propose that the TRAPP I complex is anchored, through the Bet3p subunit, to the Golgi, thus essentially lying flat on the acceptor membrane (Figure 7B). In the initial vesicle-capture step (Figure 7B, step 1), “long-distance” tethering would occur through the coiled-coil tethers such as p115 and GM130/golgin-95. The vesicle could then approach the Golgi by a bending motion in a hinge region of the coiled-coil tether, at which point it would be engaged by the TRAPP I complex (Figure 7B, step 2). Additional tethering could occur by interaction between Rab1-GTP and a cryptic Rab1-binding site on p115 that is exposed following binding to GM130/golgin-95 (Beard et al., 2005). Our EM reconstruction predicts that the two copies of the Bet3p subunit will have their putative Golgi-interacting surface oriented on the same side of the TRAPP I complex. This would result in a long, flat surface, ~65 Å wide, decorated with many conserved residues facing the cytosol (Figure 7A). Interaction of this surface with a vesicle component (Sacher et al., 2001) would then tether the vesicle to the Golgi at a distance of ~50 Å, well within the range for SNAREpin formation. Activation of Rab1/Ypt1p (Figure 7B, step 3) to recruit effector molecules followed by lateral diffusion of the TRAPP I complex from the region would then allow membrane fusion to occur.

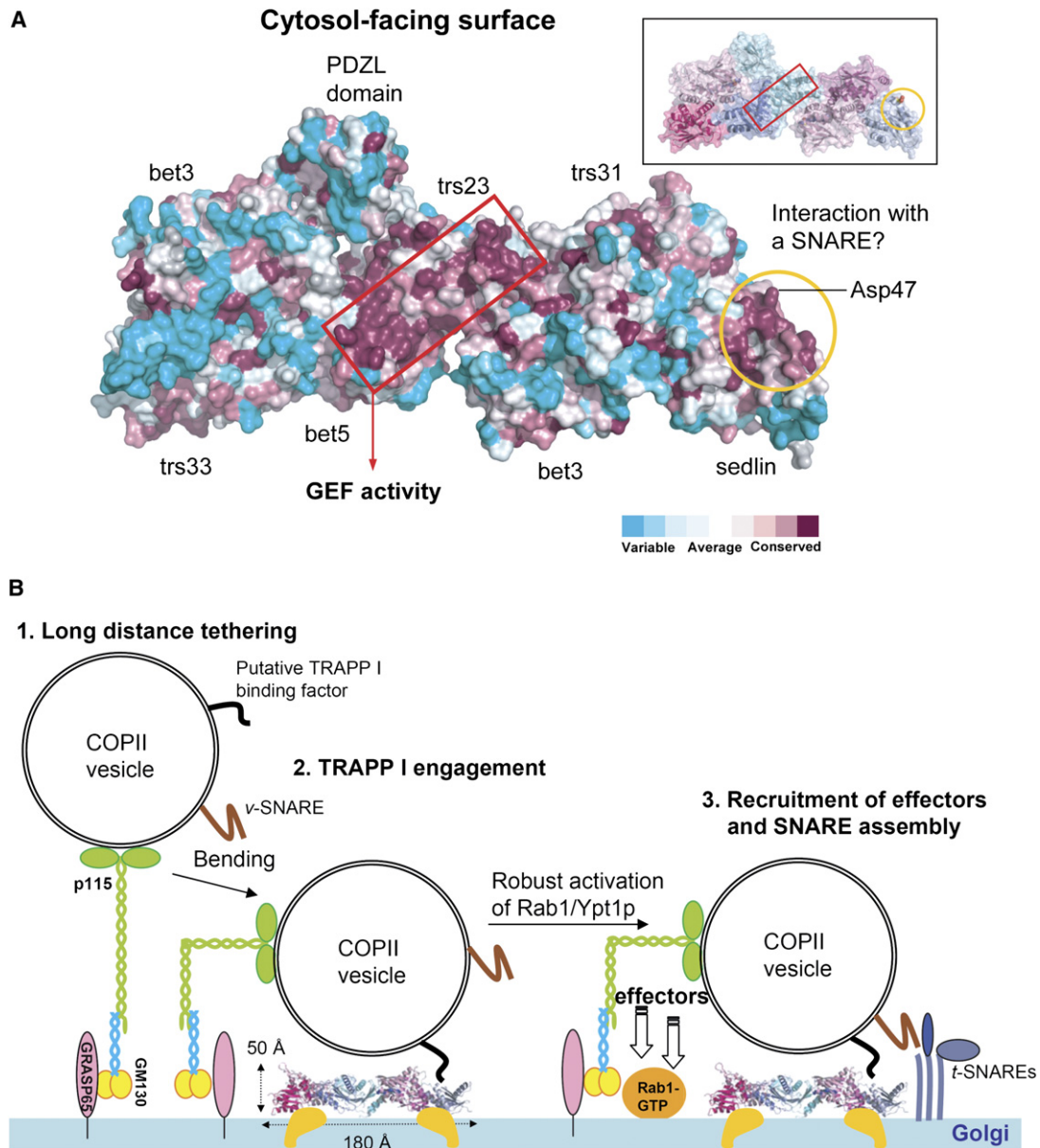


Figure 7. A Model for the Action of TRAPP I

(A) Conservation pattern calculated with ConSeq (Berezin et al., 2004) is mapped on the surface of the juxtaposed vertebrate subcomplexes representing rTRAPP I, with magenta indicating the most conserved residues and blue indicating the least conserved residues.

(B) A transport vesicle is first captured at a long distance by long, coiled-coil proteins (step 1). A bending motion in the nonhelical region of the coiled-coil protein brings the vesicle into close proximity to TRAPP I (step 2), which is anchored to the Golgi by an as yet unidentified mechanism. Upon recognition of an unidentified factor on the surface of the vesicle, the transport vesicle is more tightly tethered to the Golgi. Activation of Rab1/Ypt1p (step 3) leads to recruitment of effector molecules to eventually enable fusion. Trs20p/sedlin may facilitate or regulate the actions of the SNARE proteins. Note that the cytosol-facing surface shown in (A) is oriented upwards in (B) (i.e., rotated 90° around the x axis).

This model assumes that Rab GTPase activation/inactivation must occur at least two times during this process. Indeed, p115 has been shown to interact with ER-derived vesicles in a Rab1-GTP-dependent fashion during the budding process (Allan et al., 2000), long before the

GTPase would encounter TRAPP I. The GEF responsible for activation of the GTPase at this stage is unclear and may not be as potent as TRAPP I. Inactivation of Rab1/Ypt1p could then take place, and a conformational change in p115 (or Uso1p in yeast) would then allow it to

interact with GM130/golgin-95 at the Golgi. Once the vesicle is engaged by TRAPP I as described above, a robust activation of Rab1/Ypt1p results in the concentration of other effectors of the GTPase to the region close to the docked vesicle and the conserved surface of the complex. The spatial and temporal integration of these components by TRAPP I could then allow for the eventual fusion of the vesicle with the Golgi. This model ensures that mass recruitment of other effectors of Rab1/Ypt1p occurs only after the vesicle is in close proximity to the Golgi. This model also ensures that the vesicle does not fuse with other compartments that might otherwise occur since GM130/golgin-95 has been reported to interact with several different GTPases and could conceivably tether the vesicle to different compartments (Moyer et al., 2001; Short et al., 2001; Valsdottir et al., 2001). The distinct *cis*-Golgi localization of TRAPP I (Barrowman et al., 2000; Sacher et al., 2001) and the specificity of its GEF activity ensure that fusion will only take place at the appropriate compartment. In this respect, it is possible that the previously ascribed TRAPP GEF activity toward Ypt31p and Ypt32p (Jones et al., 2000) may reside in the unique TRAPP II subunits Trs120p and/or Trs130p.

Implications for the Disorder SEDL

Mutations in the human trs20/sedlin protein have been implicated in the etiology of the skeletal disorder spondylo-epiphyseal dysplasia late onset (SEDL) (Gedeon et al., 1999). The crystal structure of this protein shows similarity to the N-terminal regulatory domains of the SNARE proteins Ykt6p and Sec22b (Jang et al., 2002). These domains have been termed longin domains and are found in several other proteins. A recent report (Schlenker et al., 2006) suggested a generalized mode of interaction between longin domains and small GTPases and implied that sedlin/Trs20p might be involved in the regulation of Rab1/Ypt1p. Our results clearly show that removal of Trs20p from rTRAPP I does not significantly alter its Ypt1p GEF activity (Figure 2B), suggesting that sedlin/Trs20p is not involved in the regulation of Ypt1p function. The EM structure shows that the Trs20p subunit is found on the periphery of the TRAPP I complex, "capping" one end (Figure 6), and the pathogenic D47Y mutation remains exposed (Figure 7A). We propose that the pathogenesis of the D47Y mutation in sedlin is unrelated to TRAPP I GEF activity and likely interferes with a sedlin-protein interaction in which the interacting partner is yet to be identified. Along the α helix containing Asp47 is a highly conserved patch (Figure 7A) that corresponds to the groove of Ykt6p implicated in the binding of its SNARE helix (Tochio et al., 2001). It is tempting to suggest that sedlin might influence SNARE function or interactions on opposing membranes after engagement of the vesicle by TRAPP I. Alternatively, sedlin may be the site of SNARE engagement, and the D47Y mutation may interfere with this crucial event. Our elucidation of the architecture of TRAPP I will serve as a strong foundation to address its role in SEDL and to

identify factors that influence the function and localization of this complex.

EXPERIMENTAL PROCEDURES

Detailed experimental procedures can be found in the [Supplemental Data](#).

Protein Production

Mammalian Subcomplexes

All protein expressions were performed in *E. coli* BL21(DE3), and purifications were performed by a combination of metal-affinity, size-exclusion and ion-exchange chromatography. Subcomplexes were formed either by expressing individual proteins or heterodimers, mixing them in vitro, and purifying the subcomplex by size-exclusion chromatography or by coexpression in *E. coli*.

Yeast rTRAPP I and Subcomplexes

The open reading frames for the yeast subunits were cloned in pairs into each of the three dual-expression vectors pETDuet-1, pRSFDuet-1, and pACYCDuet-1 (Novagen). The vectors were sequentially transformed into *E. coli* BL21(DE3), and expression was induced with 1 mM IPTG at room temperature overnight. The complexes were purified by a combination of metal-affinity chromatography and size-exclusion chromatography.

Crystallization, X-Ray Data Collection, and Structure Determination

The bet3-trs31-sedlin crystals grew from a mixture of 20% (w/v) PEG3350, 0.2 M MgCl₂, 2% (w/v) benzamidine, and 0.1 M Tris-HCl (pH 8.0), and the bet3-trs33-bet5-trs23 crystals grew from a mixture of 20% (w/v) PEG3350, 0.28 M lithium sulfate, and 0.1 M Tris-HCl (pH 8.5). The bet3-trs33-bet5-trs23 structures were solved with SAD phasing using the programs SOLVE (Terwilliger and Berendzen, 1999) and RESOLVE (Terwilliger, 2000) with the use of the crystals of the selenomethionine-substituted proteins (Table S1). The bet3-trs31-sedlin structure was determined by molecular replacement with the CCP4 version of MOLREP (CCP4, 1994) using the structures of bet3-trs31 and sedlin as search models.

GST Pull-down Assay

Mouse bet5, trs23, and sedlin were produced as GST fusion proteins. The fusion protein was prebound to glutathione agarose and incubated with the purified proteins or subcomplexes indicated, and bound protein was detected by SDS-PAGE.

GEF Assays

Assays were performed as described previously (Jones et al., 2000; Wang et al., 2000) using 0.1–0.5 μ M rTRAPP I or subcomplexes.

Electron Microscopy and Image Processing

Protein samples (0.01 mg/ml) were negatively stained with uranyl formate as described (Ohi et al., 2004), and single-particle reconstructions were calculated using the random conical tilt approach (Radermacher et al., 1987).

Fab Labeling

Polyclonal antibodies against Trs33p were used to generate and purify Fab fragments. Labeling was performed by incubating rTRAPP I with Fab fragments at molar ratios ranging from 1:4 to 1:8 for 1 hr at 4°C in 20 mM Tris-HCl (pH 8.5), 200 mM NaCl, 2 mM dithiothreitol. The labeled complexes were imaged in negative stain.

Supplemental Data

Supplemental Data include Supplemental Experimental Procedures, Supplemental References, six figures, and one table and can be found

with this article online at <http://www.cell.com/cgi/content/full/127/4/817/DC1/>.

ACKNOWLEDGMENTS

We are grateful to Dr. C.-H. Kim for the zebrafish cDNA library, the staff at beamline 4A at the Pohang Accelerator Laboratory (South Korea) and the staff at beamline NW12AU at the Photon Factory (Japan). This study was supported by Creative Research Initiatives (Center for Biomolecular Recognition) of MOST/KOSEF (South Korea), Genome Canada and Genome Quebec as part of the Cell Map project, the Canadian Institutes of Health Research, and the National Institutes of Health (USA). Y.-G.K. was supported by the Brain Korea 21 program. The molecular EM facility at Harvard Medical School was established by a generous donation from the Giovanni Armenise Harvard Center for Structural Biology and is supported by National Institutes of Health grant GM62580 (to David DeRosier).

Received: July 7, 2006

Revised: August 8, 2006

Accepted: September 6, 2006

Published: November 16, 2006

REFERENCES

- Allan, B.B., Moyer, B.D., and Balch, W.E. (2000). Rab1 recruitment of p115 into a cis-SNARE complex: programming budding COPII vesicles for fusion. *Science* 289, 444–448.
- Barrowman, J., Sacher, M., and Ferro-Novick, S. (2000). TRAPP stably associates with the Golgi and is required for vesicle docking. *EMBO J.* 19, 862–869.
- Beard, M., Satoh, A., Shorter, J., and Warren, G. (2005). A cryptic Rab1-binding site in the p115 tethering protein. *J. Biol. Chem.* 280, 25840–25848.
- Berezin, C., Glaser, F., Rosenberg, J., Paz, I., Pupko, T., Fariselli, P., Casadio, R., and Ben-Tal, N. (2004). ConSeq: the identification of functionally and structurally important residues in protein sequences. *Bioinformatics* 20, 1322–1324.
- Cai, H., Zhang, Y., Pypaert, M., Walker, L., and Ferro-Novick, S. (2005). Mutants in trs120 disrupt traffic from the early endosome to the late Golgi. *J. Cell Biol.* 171, 823–833.
- CCP4 (Collaborative Computation Project, Number 4) (1994). The CCP4 suite: programs for protein crystallography. *Acta Crystallogr. D Biol. Crystallogr.* 50, 760–763.
- Cheng, Y., Wolf, E., Larvie, M., Zak, O., Aisen, P., Grigorieff, N., Harrison, S.C., and Walz, T. (2006). Single particle reconstructions of the transferrin-transferrin receptor complex obtained with different specimen preparation techniques. *J. Mol. Biol.* 355, 1048–1065.
- Ethell, I.M., Hagihara, K., Miura, Y., Irie, F., and Yamaguchi, Y. (2000). Synbindin, A novel syndecan-2-binding protein in neuronal dendritic spines. *J. Cell Biol.* 151, 53–68.
- Gedeon, A.K., Colley, A., Jamieson, R., Thompson, E.M., Rogers, J., Sillence, D., Tiller, G.E., Mulley, J.C., and Gecz, J. (1999). Identification of the gene (SEDL) causing X-linked spondyloepiphyseal dysplasia tarda. *Nat. Genet.* 22, 400–404.
- Gerst, J.E. (1999). SNAREs and SNARE regulators in membrane fusion and exocytosis. *Cell. Mol. Life Sci.* 55, 707–734.
- Hanson, P.I., Roth, R., Morisaki, H., Jahn, R., and Heuser, J.E. (1997). Structure and conformational changes in NSF and its membrane receptor complexes visualized by quick-freeze/deep-etch electron microscopy. *Cell* 90, 523–535.
- Jang, S.B., Kim, Y.G., Cho, Y.S., Suh, P.G., Kim, K.H., and Oh, B.H. (2002). Crystal structure of SEDL and its implications for a genetic disease spondyloepiphyseal dysplasia tarda. *J. Biol. Chem.* 277, 49863–49869.
- Jiang, Y., Scarpa, A., Zhang, L., Stone, S., Feliciano, E., and Ferro-Novick, S. (1998). A high copy suppressor screen reveals genetic interactions between BET3 and a new gene. Evidence for a novel complex in ER-to-Golgi transport. *Genetics* 149, 833–841.
- Jones, S., Newman, C., Liu, F., and Segev, N. (2000). The TRAPP complex is a nucleotide exchanger for Ypt1 and Ypt31/32. *Mol. Biol. Cell* 11, 4403–4411.
- Kim, M.S., Yi, M.J., Lee, K.H., Wagner, J., Munger, C., Kim, Y.G., Whiteway, M., Cygler, M., Oh, B.H., and Sacher, M. (2005a). Biochemical and crystallographic studies reveal a specific interaction between TRAPP subunits Trs33p and Bet3p. *Traffic* 6, 1183–1195.
- Kim, Y.G., Sohn, E.J., Seo, J., Lee, K.J., Lee, H.S., Hwang, I., Whiteway, M., Sacher, M., and Oh, B.H. (2005b). Crystal structure of bet3 reveals a novel mechanism for Golgi localization of tethering factor TRAPP. *Nat. Struct. Mol. Biol.* 12, 38–45.
- Lowe, M. (2000). Membrane transport: tethers and TRAPPs. *Curr. Biol.* 10, R407–R409.
- Moyer, B.D., Allan, B.B., and Balch, W.E. (2001). Rab1 interaction with a GM130 effector complex regulates COPII vesicle cis-Golgi tethering. *Traffic* 2, 268–276.
- Noury, C., Grant, S.G., and Borg, J.P. (2003). PDZ domain proteins: plug and play!. *Sci. STKE* 2003, RE7.
- Ohi, M., Li, Y., Cheng, Y., and Walz, T. (2004). Negative Staining and Image Classification - Powerful Tools in Modern Electron Microscopy. *Biol. Proced. Online* 6, 23–34.
- Pfeffer, S.R. (1996). Transport vesicle docking: SNAREs and associates. *Annu. Rev. Cell Dev. Biol.* 12, 441–461.
- Radermacher, M., Wagenknecht, T., Verschoor, A., and Frank, J. (1987). Three-dimensional reconstruction from a single-exposure, random conical tilt series applied to the 50S ribosomal subunit of *Escherichia coli*. *J. Microsc.* 146, 113–136.
- Sacher, M., Jiang, Y., Barrowman, J., Scarpa, A., Burston, J., Zhang, L., Schieltz, D., Yates, J.R., III, Abeliovich, H., and Ferro-Novick, S. (1998). TRAPP, a highly conserved novel complex on the cis-Golgi that mediates vesicle docking and fusion. *EMBO J.* 17, 2494–2503.
- Sacher, M., Barrowman, J., Schieltz, D., Yates, J.R., III, and Ferro-Novick, S. (2000). Identification and characterization of five new subunits of TRAPP. *Eur. J. Cell Biol.* 79, 71–80.
- Sacher, M., Barrowman, J., Wang, W., Horecka, J., Zhang, Y., Pypaert, M., and Ferro-Novick, S. (2001). TRAPP I implicated in the specificity of tethering in ER-to-Golgi transport. *Mol. Cell* 7, 433–442.
- Schlenker, O., Hendricks, A., Sinning, I., and Wild, K. (2006). The structure of the mammalian signal recognition particle (SRP) receptor as prototype for the interaction of small GTPases with Longin domains. *J. Biol. Chem.* 281, 8898–8906.
- Short, B., Preisinger, C., Korner, R., Kopajtich, R., Byron, O., and Barr, F.A. (2001). A GRASP55-rab2 effector complex linking Golgi structure to membrane traffic. *J. Cell Biol.* 155, 877–883.
- Terwilliger, T.C. (2000). Maximum-likelihood density modification. *Acta Crystallogr. D Biol. Crystallogr.* 56, 965–972.
- Terwilliger, T.C., and Berendzen, J. (1999). Automated MAD and MIR structure solution. *Acta Crystallogr. D Biol. Crystallogr.* 55, 849–861.
- Tochio, H., Tsui, M.M., Banfield, D.K., and Zhang, M. (2001). An auto-inhibitory mechanism for nonsyntaxin SNARE proteins revealed by the structure of Ykt6p. *Science* 293, 698–702.
- Tong, A.H., Evangelista, M., Parsons, A.B., Xu, H., Bader, G.D., Page, N., Robinson, M., Raghibizadeh, S., Hogue, C.W., Bussey, H., et al. (2001). Systematic genetic analysis with ordered arrays of yeast deletion mutants. *Science* 294, 2364–2368.

Turnbull, A.P., Kummel, D., Prinz, B., Holz, C., Schultchen, J., Lang, C., Niesen, F.H., Hofmann, K.P., Delbruck, H., Behlke, J., et al. (2005). Structure of palmitoylated BET3: insights into TRAPP complex assembly and membrane localization. *EMBO J.* *24*, 875–884.

Valsdottir, R., Hashimoto, H., Ashman, K., Koda, T., Storrie, B., and Nilsson, T. (2001). Identification of rabaptin-5, rabex-5, and GM130 as putative effectors of rab33b, a regulator of retrograde traffic between the Golgi apparatus and ER. *FEBS Lett.* *508*, 201–209.

Wang, W., Sacher, M., and Ferro-Novick, S. (2000). TRAPP stimulates guanine nucleotide exchange on Ypt1p. *J. Cell Biol.* *151*, 289–296.

Waters, M.G., and Hughson, F.M. (2000). Membrane tethering and fusion in the secretory and endocytic pathways. *Traffic* *1*, 588–597.

Weber, T., Zemelman, B.V., McNew, J.A., Westermann, B., Gmachl, M., Parlati, F., Sollner, T.H., and Rothman, J.E. (1998). SNAREpins: minimal machinery for membrane fusion. *Cell* *92*, 759–772.

Whyte, J.R., and Munro, S. (2002). Vesicle tethering complexes in membrane traffic. *J. Cell Sci.* *115*, 2627–2637.

Accession Numbers

The coordinates of the bet3-trs31, bet-trs31-sedlin, and bet3-trs33-bet5-trs23 structures have been deposited in the Protein Data Bank with the ID codes 2J3R, 2J3W, and 2J3T, respectively.

Supplemental Data

The Architecture of the Multisubunit

TRAPP I Complex Suggests

a Model for Vesicle Tethering

Yeon-Gil Kim, Stefan Raunser, Christine Munger, John Wagner, Young-Lan Song, Miroslaw Cygler, Thomas Walz, Byung-Ha Oh, and Michael Sacher

Supplemental Experimental Procedures

Protein Production – Mammalian Subcomplexes

The coding sequences for mouse bet3 and zebrafish trs31 were cloned into the pProExHTa (Invitrogen) and the pET30a vector (Novagen), respectively. *Escherichia coli* BL21 (DE3) cells, transformed with the two plasmids, were used to produce the bet3-trs31 heterodimer. The heterodimer was purified by using Ni-NTA (Qiagen), Mono Q and Superdex 200 (GE Healthcare) columns. Sedlin was produced from pET15b and purified as described (Jang et al., 2002). The bet3-trs31-sedlin subcomplex was prepared by mixing the bet3-trs31 heterodimer and sedlin at equal molar ratio. The protein mixture was loaded on a Hiload 26/60 Superdex 200 column to separate uncomplexed protein from the trimeric subcomplex. The final purified complex was concentrated to 12 mg/ml in buffer A composed of 10 mM Tris-HCl (pH 8.0) and 200 mM sodium chloride, and used for crystallization. Each of the coding sequences for mouse bet5 and human trs23 was first cloned into the pET30a vector, and subsequently a two-promoter expression vector constructed, in which both bet5 and trs23 were under the control of T7 promoter. The other two-promoter vector harboring mouse bet3 and human trs33 genes was constructed as reported previously (Kim et al., 2005a). *E. coli* BL21 (DE3) cells transformed with these vectors were used to produce the bet3-trs33-bet5-trs23 subcomplex. The subcomplex was purified by using the same protocol for the purification of bet3-trs31. The purified subcomplex was concentrated to 20 mg/ml in buffer A.

The selenomethionine-substituted bet3-trs31 and bet3-trs33-bet5-trs23 were produced in *E. coli* B834 (DE3) methionine auxotroph (Novagen) and purified as described above.

Protein Production – Yeast rTRAPP I and Subcomplexes

The open reading frames for the yeast subunits Bet3p, Bet5p, Trs20p, Trs23p, Trs31p and Trs33p were amplified by PCR, incorporating a hexahistidine tag into the forward primer for Bet3p, and cloned in pairs into each of the three dual-expression vectors pETDuet-1 (Amp^R), pRSFDuet-1 (Kan^R) and pACYCDuet-1 (Cam^R) (Novagen). To express subcomplexes of three or more subunits, the relevant vectors were sequentially transformed into *E. coli* BL21(DE3) and expression was induced with 1 mM IPTG at room temperature overnight. The complexes were purified first by metal affinity chromatography using Ni-NTA and the protein concentration was

determined. Approximately 5 mg of Ni-NTA-purified material was further purified by size exclusion chromatography as described below. For stoichiometric determinations, scanned gels were analyzed using ImageQuant software (version 5.2) (Molecular Dynamics) and errors were no more than +/-15%.

Crystallization, X-Ray Data Collection and Structure Determination

The bet3-trs31 crystals grew from a mixture of 0.26 M ammonium nitrate and 14% (w/v) polyethylene glycol monomethyl ether 5000; the bet3-trs31-sedlin crystals from a mixture of 20% (w/v) PEG3350, 0.2 M MgCl₂, 2% (w/v) benzamidine and 0.1 M Tris HCl (pH 8.0); the bet3-trs33-bet5-trs23 crystals from a mixture of 20% (w/v) PEG 3350, 0.28 M lithium sulfate and 0.1 M Tris HCl (pH 8.5). All of the crystals were grown by sitting-drop vapor diffusion method at 20°C by mixing and equilibrating 2.5 µl of each of the protein solution and the respective precipitant solution. The bet3-trs31 and bet3-trs33-bet5-trs23 structures were solved with SAD phasing by using the programs SOLVE (Terwilliger and Berendzen, 1999) and RESOLVE (Terwilliger, 2000) with the use of the crystals of the selenomethionine-substituted proteins (Supplementary Table 1). The bet3-trs31-sedlin structure was determined by molecular replacement with the CCP4 version of MOLREP (CCP4, 1994) using the structure of bet3-trs31 and sedlin as search models. All diffraction data were processed using the HKL2000 package (Otwinowski and Minor, 1997). Model building and refinements were performed using program O (Jones et al., 1991) and CNS (Brunger et al., 1998), respectively.

GST Pull-down Assay

The GST-bet5, GST-sedlin and trs23-GST proteins were produced in *E. coli* BL21(DE3) using the pGEX4T3 (GE Healthcare) or pET30a vector (Novagen). The proteins were purified with GST-bind resin (Novagen) and further purified with a Hitrap Q column. 100 µg of the purified GST-bet5, GST-sedlin or trs23-GST protein was allowed to bind to glutathione-agarose resin in 1ml of PBS buffer and then incubated with each of 100 µg of purified bet3, bet5, sedlin, trs23, trs33, bet3-trs33 and bet3-trs31 for 1 h with gentle shaking at 4°C. After washing the resin five times with PBS buffer, the resin-bound proteins were eluted and detected by SDS-PAGE and Coomassie blue staining.

Gel Filtration

Each of 10 nmoles of the purified proteins (bet5, sedlin, trs23, bet3-trs31, bet3-trs33) was loaded onto a HiLoad 26/60 Superdex 200 column equilibrated with a buffer solution containing 30 mM TrisHCl (pH 8.0) and 100 mM NaCl. Peak fractions were analyzed by SDS-PAGE. On the same column, loaded was ~ 1.2 mg of the mixture of bet3-trs31 and sedlin (at 1:1 molar ratio), bet3-trs33 and bet5 (at 1:2 molar ratio) or bet3-trs33-bet5 and trs23 (at 1:2 molar ratio). The purified yeast heteromeric complexes (Bet3p-Trs31p-Trs20p, Bet3p-Trs33p-Bet5p, Bet3p-Trs33p-Bet5p-Trs23p) were analyzed on an analytical Superdex 200 column equilibrated with a buffer solution containing 20 mM Tris (pH 8.5), 200 mM NaCl and 5 mM DTT. rTRAPP I was purified on a HiLoad 16/60 Superdex 200 column equilibrated with the same buffer as the analytical column.

Yeast Techniques

Standard techniques and media were used for the growth of the yeast cells and dissection of the tetrads (Guthrie and Fink, 1991).

Mutagenesis

All of the mutants used in this study were generated using the QuikChange kit (Stratagene).

Electron Microscopy and Image Processing

Electron micrographs were recorded at an acceleration voltage of 120 kV. Image pairs were collected at tilt angles of 60° and 0°. 9,417 rTRAPP I particle pairs were selected from 27 image pairs using WEB, the display program associated with the SPIDER software package (Frank et al., 1996), which was used for further image processing steps. The particle images from the untilted specimen were subjected to ten cycles of multireference alignment and K-means classification specifying 100 output classes. Representative class averages are shown in Fig. 6B. The differences seen between individual class averages may represent a different level of stain embedding, rotation of the particle about its long axis or slight conformational changes. We then merged three classes that produced very similar averages (about 1,900 particle pairs). The images from the tilted specimen were used to calculate a 3D reconstruction by back-projection, back-projection refinement and angular refinement in SPIDER. Further refinement of the volume and correction for the contrast transfer function (CTF) of the electron microscope was done with FREALIGN (Stewart and Grigorieff, 2004). The defocus value of each particle in an image of a tilted specimen, needed for CTF correction, was deduced from the position of the particle in the image with respect to the tilt axis and the defocus value of the image, which was determined with CTFTILT (Mindell and Grigorieff, 2003). The final volume obtained by angular refinement with SPIDER was used as reference model, to which the particles selected from both the images of the tilted and untilted specimen were aligned with FREALIGN. Fourier shell correlation (FSC) curves indicated a resolution of 30 Å using the FSC=0.5 criterion and a resolution of 26 Å using the FSC=0.142 criterion (Rosenthal and Henderson, 2003).

Supplemental References

- Brunger,A.T., Adams,P.D., Clore,G.M., DeLano,W.L., Gros,P., Grosse-Kunstleve,R.W., Jiang,J.S., Kuszewski,J., Nilges,M., Pannu,N.S., Read,R.J., Rice,L.M., Simonson,T., and Warren,G.L. (1998). Crystallography & NMR system: A new software suite for macromolecular structure determination. *Acta Crystallogr. D. Biol. Crystallogr.* *54*, 905-921.
- CCP4 (1994). The CCP4 suite: programs for protein crystallography. *Biol. Crystallogr.* *50*, 760-763.
- Frank,J., Radermacher,M., Penczek,P., Zhu,J., Li,Y., Ladjadj,M., and Leith,A. (1996). SPIDER and WEB: processing and visualization of images in 3D electron microscopy and related fields. *J. Struct. Biol.* *116*, 190-199.
- Guthrie,C. and Fink,G.R. (1991). Guide to yeast genetics and molecular biology. in *Meth. Enzymol.* *194*, Academic Press, USA.
- Jang,S.B., Kim,Y.G., Cho,Y.S., Suh,P.G., Kim,K.H., and Oh,B.H. (2002). Crystal structure of SEDL and its implications for a genetic disease spondyloepiphyseal dysplasia tarda. *J. Biol. Chem.* *277*, 49863-49869.
- Jones,T.A., Zou,J.Y., Cowan,S.W., and Kjeldgaard (1991). Improved methods for building protein models in electron density maps and the location of errors in these models. *Acta Crystallogr. A* *47 (Pt 2)*, 110-119.
- Kim,M.S., Yi,M.J., Lee,K.H., Wagner,J., Munger,C., Kim,Y.G., Whiteway,M., Cygler,M., Oh,B.H., and Sacher,M. (2005). Biochemical and crystallographic studies reveal a specific interaction between TRAPP subunits Trs33p and Bet3p. *Traffic.* *6*, 1183-1195.
- Mindell,J.A. and Grigorieff,N. (2003). Accurate determination of local defocus and specimen tilt in electron microscopy. *J. Struct. Biol.* *142*, 334-347.
- Otwinowski,Z. and Minor,W. (1997). Processing of x-ray diffraction data collected in oscillation mode. *Methods Enzymol.* *276*, 307-326.
- Rosenthal,P.B. and Henderson,R. (2003). Optimal determination of particle orientation, absolute hand, and contrast loss in single-particle electron cryomicroscopy. *J. Mol. Biol.* *333*, 721-745.
- Stewart,A. and Grigorieff,N. (2004). Noise bias in the refinement of structures derived from single particles. *Ultramicroscopy* *102*, 67-84.
- Terwilliger,T.C. (2000). Maximum-likelihood density modification. *Acta Crystallogr. D. Biol. Crystallogr.* *56*, 965-972.
- Terwilliger,T.C. and Berendzen,J. (1999). Automated MAD and MIR structure solution. *Acta Crystallogr. D. Biol. Crystallogr.* *55*, 849-861.

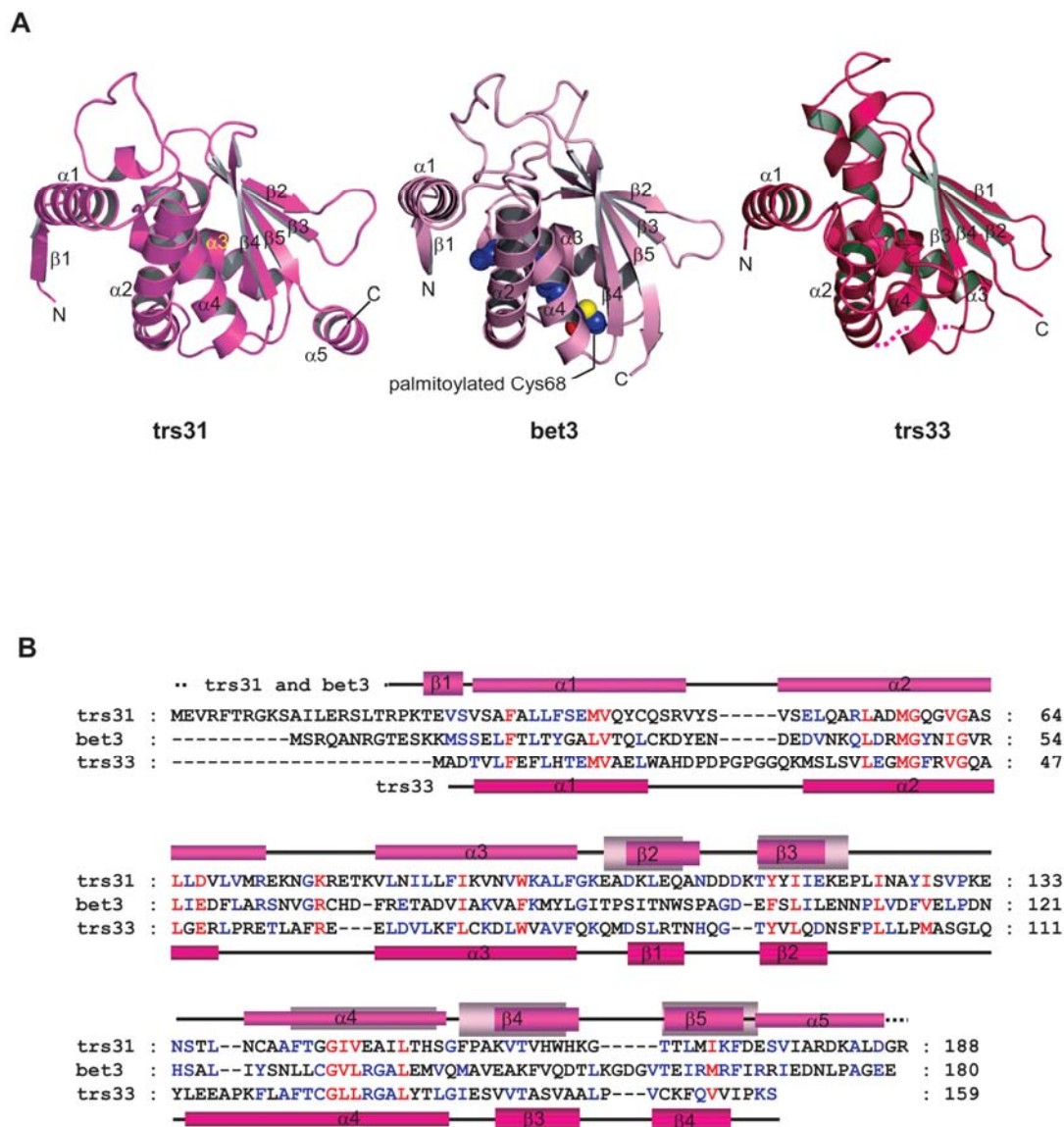



Figure S1. Structural Similarity and Sequence Alignment of the bet3 Family Members


(A) Comparison of the bet3 structural homologs. The monomeric structures of zebrafish trs31, mouse bet3 and human trs33 are shown in the same orientations. Dotted lines represent disordered residues.

(B) Sequence alignment and secondary structure assignments of zebrafish trs31, mouse bet3 and human trs33. The red and blue letters indicate the amino acids that are conserved in all or two of the three proteins, respectively. The secondary structural elements of trs31 and trs33 are represented above and below the aligned sequences, respectively, as cylinders for α -helices and arrows for β -strands. The secondary structures of bet3 are shown in pink only when they are different from those of trs31. GenBank accession numbers are trs31, NM_001002482; bet3, AAH78259 and trs33, AAC62259.

.....


10 20 30 40 50

H.sapi. : -MEARFTRGKSALLERALARPR-TEVSLSAFALLFSELVQHCQSRVFSVAELQSRLAALG : 58
M.musc. : -MEARFTRGKSALLERALVRPR-TEVSLSAFALLFSELVQHCQSRVFSVAELQARLAALG : 58
G.gall. : -MESRFTRGKSPLLERPLGRPR-GEVSLSAFALLFCELVQYCQRRVYSVAELQSKLAQLG : 58
D.reri. : -MEVRFTRGKSAILERSLTRPK-TEVSVSAFALLFSEMVQYCQSRVYSVSELQARLADMG : 58
X.laev. : -MDSRFSRGKSSILERSLARPK-TEVSLSAFALLFSEIVQYCQNRVYSVSELQAKLSELG : 58
D.mela. : -LKISSMRPRSNIIDRPLSKGK-TEVSQSIVALLFSEIVQYSQSRVFTVPELQTRLHDLG : 64
C.eleg. : -----MAKTGTILDKSLSRGK-TEINLSTFAVLFSSEMVLYAQNRSETVTDIHDKIASYG : 53
S.pomb. : -LKSTAPLMGKSVYEQNLNKIRNSDVNLSSFAFIFSELIQRIQSQVSGIQEFEEKLNEHG : 75
S.cere. : -SEASTTYIPSRITYSESLLFKR-QEASLSAMAFLFQEMISQLHRTCKTAGDFETKLSDYG : 91




60 70 80 90 100 110

H.sapi. : RQVGARVLDALVARE-----KGARRETQVLGALLFVKGAVWKALFGKEADKLEQANDDA : 112
M.musc. : RQVGARVLDALVARE-----KGARRETQVLGALLFVKGAVWKALFGKEADKLEQANDDA : 112
G.gall. : HQVGLRLLDPLVSRE-----RGGRRRETQVLSVLLFVKGPVWRALFGKEADKLEQANDDD : 112
D.reri. : QGVGASLLDVLVRE-----KNGKRETQVLNILLFIKVNWKALFGKEADKLEQANDDD : 112
X.laev. : QQVGCRLLDPLVRE-----KNGKRETQVISALLFIKVVWKALFGKEADKLEQANDDD : 112
D.mela. : QDVGTRIIDLIFVRE-----RSSKRETQKLQMLLFVKTWKNLFGKEAEKLEHANDDE : 118
C.eleg. : KQVGLRMFDIITLRE-----KGYKRETQKLLGMLFIKSTVWKNLFGKEADKLEERSNDDH : 107
S.pomb. : YRVGQKLVELVWRE-----RNPKRETRILGILQYIHSSVWKYLFKGKHADSLEKSKEAS : 129
S.cere. : HNIGIRLLELLNFRA-(60)-KMRRLDLKILDILQFIHGTLSYLFNHVSDDLKVKSSERD : 206



120 130 140 150 160

H.sapi. : RTFYIIEREPLINTYISVPKENSTLNCASFAGIVEAVLTHSGFPAKVTAH-----WHK : 166
M.musc. : RTFYIIEREPLINTYISVPKENSTLNCASFAGIVEAVLTHSGFPAKVTAH-----WHK : 166
G.gall. : KTTYVIEREPLVNTFISVPRENSTLNCASFAGIVEAVLGASGFPKVTAH-----WHK : 166
D.reri. : KTTYIIKEEPLINAYISVPKENSTLNCASFAGIVEAILTHSGFPAKVTVH-----WHK : 166
X.laev. : KTTYIIKEEPLINAYISVPKENSTLNCASFAGIVESLLTCSGFPKVTAH-----WHK : 166
D.mela. : RTYYIIKEEPLVNTFISVPKDKGSLNCANFTAGIVEAVLTNCGFPCKVTAH-----WHK : 172
C.eleg. : CTYLLIEKDPVNTYISVPRDKGVLNCAFAAGIVEAILESASFCKKVTAH-----WHN : 161
S.pomb. : DEYMIVDNNPLLNKFISVPKEMNQLNCCAYLAGIIEGFLDSAQFPCKASAHSVPLSQYPY : 189
S.cere. : NEYMIVDNFPTLTQFI---PGENVSCFYVCGIIGKFLFNAGFPKGVTAHRMPQGHSQ : 262



170 180

H.sapi. : GTTLMIKFEEAVIARDRALEGR : 188
M.musc. : GTTLMIKFEEAVIARDRALEGR : 188
G.gall. : GTTLMIKFEEGVARDKSLEGR : 188
D.reri. : GTTLMIKFDESVIARDKALDGR : 188
X.laev. : GTTLMIKFDESVIARDKALDGR : 188
D.mela. : GTTYMVKFEDFVIARDKQMEER : 194
C.eleg. : GTAYVIQFDESVIARENSLLDSNR : 185
S.pomb. : RTVILIKLDPSVIAREEVLG : 209
S.cere. : RTVYLIQFDRQVLDREGLRFG : 283

Figure S2. Sequence Alignment of trs31 Orthologs

Secondary structure assignment and sequence alignment of trs31. The red and blue letters indicate the amino acids that are 100% and >70% conserved in nine representative trs31 orthologs. Secondary structural elements of trs31 are indicated above the alignment. The filled circles below the sequences denote the basic residues on the putative membrane interacting surface of the bet3-trs31 heterodimer. The GenBank accession numbers for the trs31 sequences are *H.sapi.* (Homo sapiens, AAH42161), *M.musc.* (Mus musculus, NP_079977), *G.gall.* (Gallus gallus, CAH65425), *D.reri.* (Dario rerio, NP_956955), *X.laev.* (Xenopus laevis, AAH76644), *D.mela.* (Drosophila melanogaster, NP_610986), *C.eleg.* (Caenorhabditis elegans, NP_496593), *S.pomb.* (Schizosaccharomyces pombe, NP_596451) and *S.cere.* (Saccharomyces cerevisiae, NP_010760).

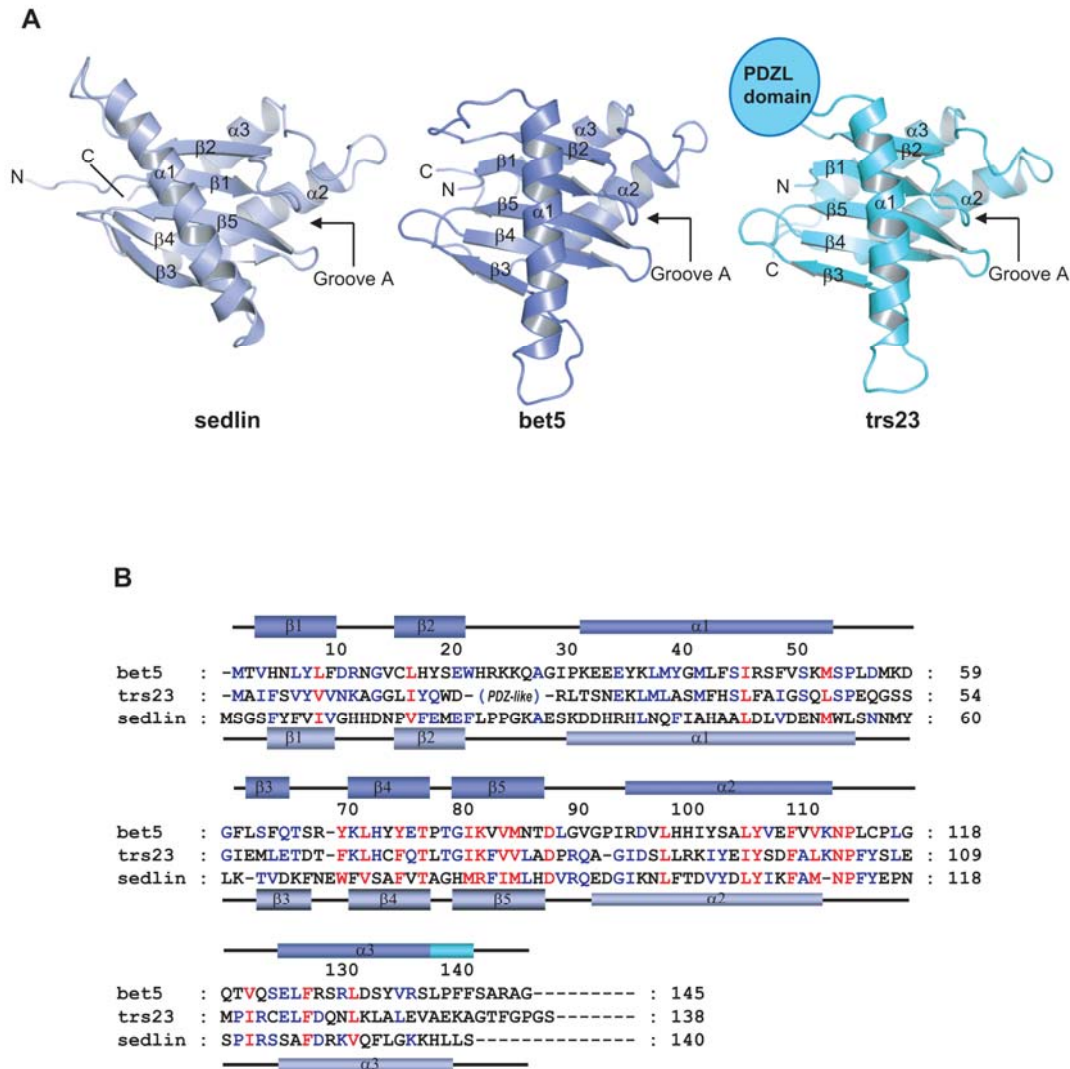


Figure S3. Structural Similarity and Sequence Alignment of the Sedlin Family Members

(A) Comparison of the sedlin structural homologues. The structures of sedlin (in the trimeric subcomplex), bet5 and the sedlin-like domain of trs23 are shown in the same orientations. Helix $\alpha 1$ of sedlin is more tilted relative to the β -sheet compared with $\alpha 1$ of bet5 or trs23. Notably, the tilt angle is very close to that observed for the N-terminal regulatory domain of Ykt6p (PDP ID: 1IOU) or mSec22b (PDP ID: 1IFQ).

(B) Sequence alignment and secondary structure assignments of bet5, sedlin and the sedlin-like domain of trs23. The red and blue letters indicate the amino acids that are conserved in all or two of the three proteins, respectively. The secondary structural elements of bet5 and sedlin are represented above and below the aligned sequences, respectively, as cylinders for α -helices and arrows for β -strands. The secondary structures of trs23 are shown in aquamarine only when they are different from those of bet5. GenBank accession numbers are bet5, NM_001002482; sedlin, AAH78259 and trs23, AAC62259.

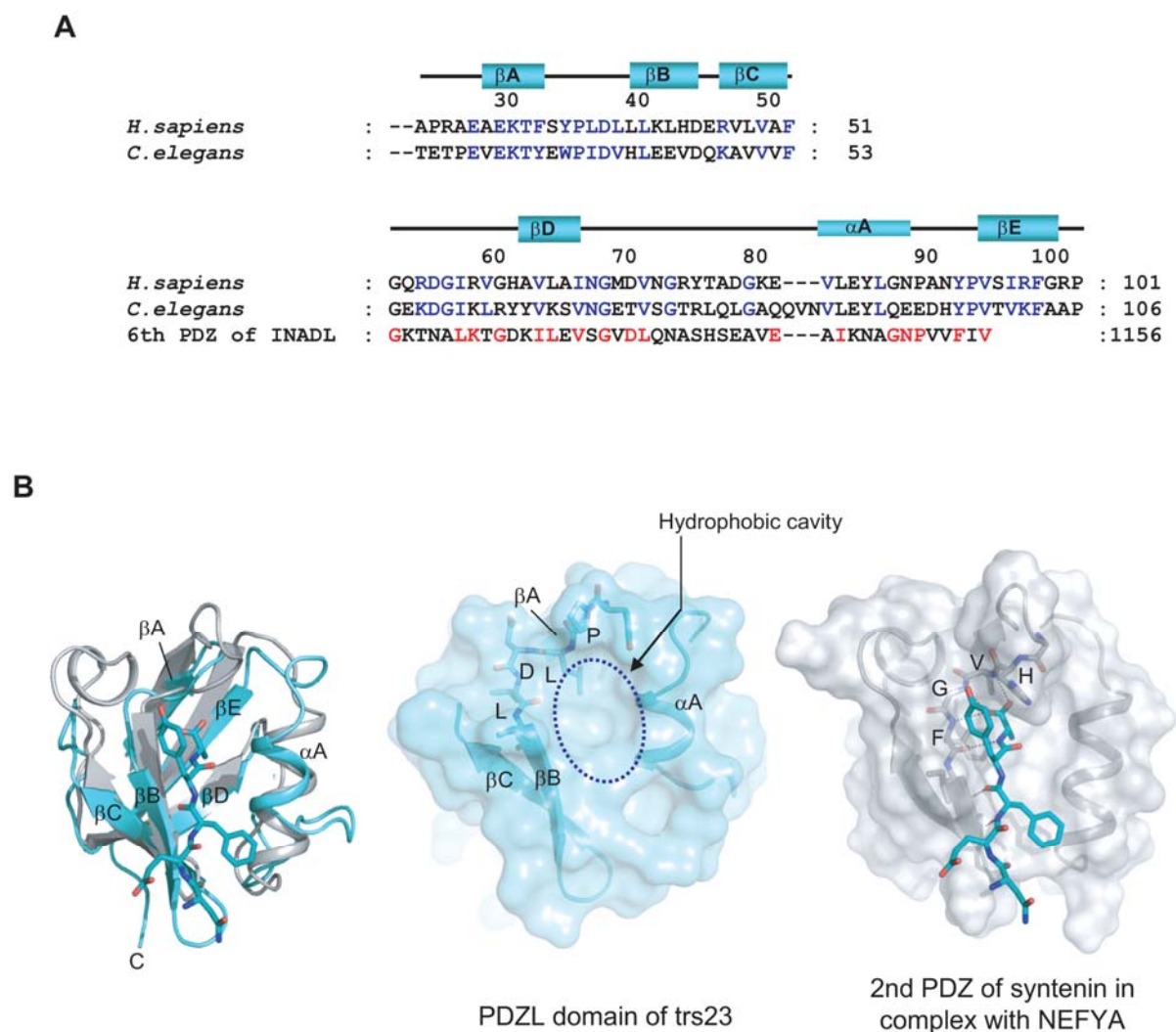


Figure S4. Comparison of the PDZL Domain of trs23 with a Classical PDZ Domain

(A) Sequence comparison. The sequences of the PDZL domain of human trs23, worm trs23 and the 6th PDZ domain of INADL (accession code: AC097064) are aligned. The blue and red letters indicate the amino acids that are conserved in metazoan trs23 orthologs and between the PDZL domain of human trs23 and the 6th PDZ domain of INADL, respectively.

(B) Comparison of the PDZL domain of trs23 with a PDZ domain of syntenin. The structure of a PDZ domain of syntenin in complex with the peptide NEFYA (PDB code: 1OBY) is shown in an orientation equivalent to that of the PDZL domain.

←

β1 β2 βA βB βC

10 20 30 40 50 60

M.musc. : --MAIFS**VYV**VN**KAGGLIYQ**WDSYSPRAEAE**KTF**SYPLDLLLKLHDERVLVAF**GQ**RDGIRVGH : 61

H.sapi. : --MAIFS**VYV**VN**KAGGLIYQ**LSYAPRAEAE**KTF**SYPLDLLLKLHDERVLVAF**GQ**RDGIRVGH : 61

G.gall. : --MAIFS**VYV**VN**KAGGLIYQ**LHDYAPRSD**EMTF**SYPLDLVLRPRDERVVVAF**GQ**RDGIRVGH : 61

D.reri. : --MAIFS**VYV**VN**KAGGLIYQ**YDNYVPRAEVE**KTF**SFPLDLVLKIHDEKVVVS**FQ**RDGIRVGH : 61

X.laev. : --MAIFS**VYV**VN**KAGGLIYQ**LDNQSPRSETE**KTF**SFPLDLVLKVHDERVIVS**FQ**RDGIRVGH : 61

D.mela. : --MI**IYGVYIVSKSGGLIF**NLDNNVPRIEHE**KTF**TYPLDLVLDYDSK**KVS**VSFNRKDGINVGH : 61

C.eleg. : MSNHI**QHLFIINRAGSLIY**SWEARTETPEVE**KTYEWP**IDVHLEEVDQ**KAVVV**GEKDGIKRLRY : 63

S.pomb. : ----**MHALIIINRAGSLIFQ**REFGS----- : 21

S.cere. : --MA**ETILVINKSGGLIYQ**RNFTN----- : 23

PDZL domain →

βD αA βE α1

70 80 90 100 110 120

M.musc. : AVLAINGMDVNGKYTADGKE---VLEYLGNPANYPVSIRFGRPRLTS**NEKML**ASMFHSLFAI : 121

H.sapi. : AVLAINGMDVNGRYTADGKE---VLEYLGNPANYPVSIRFGRPRLTS**NEKML**ASMFHSLFAI : 121

G.gall. : AVLAINGAEVNGRLTADGKD---VLEFLSNPANYPVSIRFGRHRLSS**NEKML**ASMFHSLFAI : 121

D.reri. : AVLSINGVDVNGKFTAEGKE---IQEYLRDPANYPVSIRFGRQKLSS**NEKML**ASMFHSLFAI : 121

X.laev. : AVLSINGIDVNGRYTADGKE---ILEYLGNSNYPLSIRFGRPRLTS**NEKML**ASMFHSLFAI : 121

D.mela. : VLVAVNGMPVNGVTLDGGRD---VRTTLDAPENYPINLKFSRP**KMTTNEKI**FLASMFYPLFAI : 121

C.eleg. : YVKS**VNGETVSGTRLQLGAQQVN**LEYLQEEDHYPVTVKFAAPT**VSTNEKI**ILSSMFHSLFTI : 126

S.pomb. : -----SPTALTP**NEYLV**LAGTIGHV**HAI** : 44

S.cere. : -----DEQ**KLNSNEYLI**LASTLHG**VFAI** : 46

β3 β4 β5

130 140 150 160 170

M.musc. : GS**QLS**PEQG-----SSGIEMLETD**TFKLHCFQTLTG**IKFVV**LADPRQ**-----AGID**SLLRK** : 172

H.sapi. : GS**QLS**PEQG-----SSGIEMLETD**TFKLHCYQTLTG**IKFVV**LADPRQ**-----AGID**SLLRK** : 172

G.gall. : GS**QLS**PEVG-----SSGIEMLETD**TFKLHCFQTLTG**IKFVV**LADPRQ**-----AGID**ALLRK** : 172

D.reri. : GS**QLS**PEVG-----SSGIEMLETD**TFKLHCFQTLTG**IKFIV**LADPRQ**-----SGID**ALLRK** : 172

X.laev. : GS**QLS**PEPG-----SSGIEMLETD**TFKLHCYQTLTG**IKFMV**LSDP**RQ-----AGID**TLLRK** : 172

D.mela. : AS**QLS**PEPK-----SSGI**EILEADTF**LHCF**QTLTG**IKF**II**SETGL-----NGID**LLRK** : 172

C.eleg. : AV**QLS**PCQK-----SSG**VEVLETTQFKLFCLQ**SR**TGVK**FVV**ITSAASN**-----IAAD**SLLSK** : 178

S.pomb. : ST**QIS**PLPG-----SSGI**QLLEAGTFNMHILQ**TH**TGMK**FV**LFTEKKT**-----TNAR**LQLQK** : 95

S.cere. : AS**QLT**PKAL- (60) -K**SGLRQLCTDQFTMFIYQTLTGLK**FVAISS**SVM**- (24) -Q**IADN**FL**RK** : 181

α2 α3

180 190 200 210

M.musc. : **IYEIYSD**FALKNPFYSLEMP**IRCE**LF**DQNLK**LALEVAEKAGTFGPGS : 219

H.sapi. : **IYEIYSD**FALKNPFYSLEMP**IRCE**LF**DQNLK**LALEVAEKAGTFGPGS : 219

G.gall. : **IYEIYSD**FALKNPFYSLEMP**IRCE**LF**DQNLK**LALEVAEKAGPFPGS : 219

D.reri. : **IYEIYSD**FALKNPFYSLEMP**IRCE**LF**DQNLK**SALEIAEKAGTFGPGS : 219

X.laev. : **IYELYSD**YALKNPFYSLEMP**IRSE**LF**DQNL**RSTLEVAEKAGTFGPSS : 219

D.mela. : **VYELYSD**YVLKNPFYSLEMP**IRCE**LF**DNKLQ**ELLAQVEKTGISNIDK : 219

C.eleg. : **MYELYTD**FALKNPFYSIDMP**IRAQK**FDEAI**KTLL**ERA**EKNNGAVTF** : 224

S.pomb. : **FYELYSD**YVLKNPFY**TTLEMP**IK**QCLFDEQ**LKRYIDSH : 132

S.cere. : **VYCLYSD**Y**VMKDP**SY**SEMP**IRSN**LFDEKVKM**V**ENLQ** : 219

Figure S5. Sequence Alignment of trs23 Orthologs

The red and blue letters indicate the amino acids that are 100% and >70% conserved in nine representative trs23 orthologs. Secondary structural elements of trs23 are indicated above the alignment. The GenBank accession numbers for the trs23 sequences are *H.sapi.* (Homo sapiens, NP_057230), *M.musc.* (Mus musculus, NP_068561), *G.gall.* (Gallus gallus, XP_417925), *D.reri.* (Dario rerio, NP_957058), *X.laev.* (Xenopus laevis, AAI06501), *D.mela.* (Drosophila melanogaster, NP_610986), *C.eleg.* (Caenorhabditis elegans, NP_505435), *S.pomb.* (Schizosaccharomyces pombe, NP_596670) and *S.cere.* (Saccharomyces cerevisiae, NP_010532).

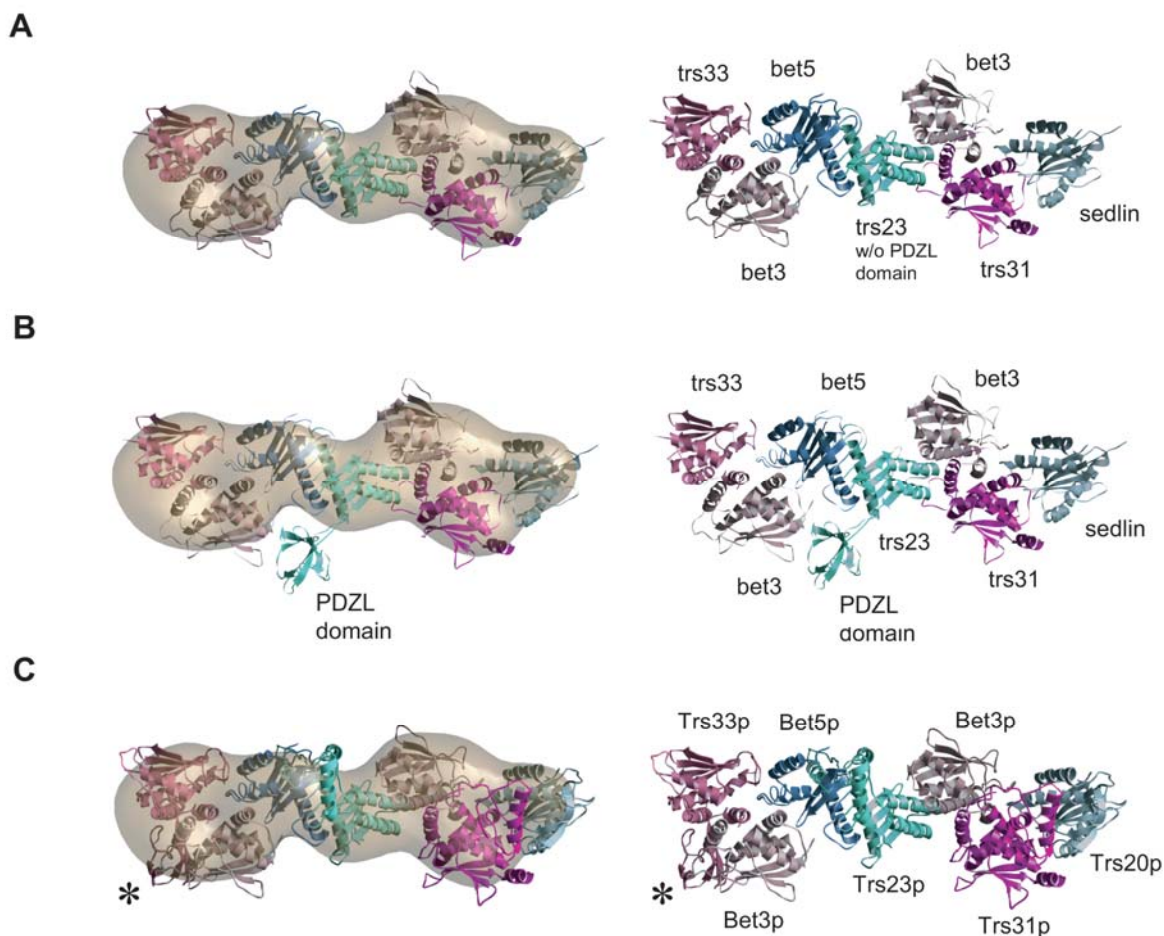


Figure S6. Comparison between the Mammalian and Yeast TRAPP I Complexes

(A) Fit of the crystal structures of the mammalian subunits into the volume of the yeast complex; the PDZL domain of trs23 was removed before fitting.

(B) Fit of the crystal structures of the complete mammalian subunits into the volume of the yeast complex, showing that the PDZL domain of trs23 protrudes from the density map.

(C) The amino acid sequences of all subunits of the yeast TRAPP I complex were aligned manually to their mammalian homologs, and the program SWISS-MODEL was used to calculate homology models for the yeast proteins based on the crystal structures of the mammalian proteins. The homology models were fit into the volume of the yeast complex. The asterisk in panel C indicates the putative binding site of the Fab fragment on Trs33p.

Table S1. Data Collection, Phasing, and Refinement Statistics

	bet3-trs33-bet5-trs23	bet3-trs33-bet5-trs23 (Selenomethione)	bet3-trs31	bet3-trs31 (Selenomethione)	bet3-trs31-Sedlin
Data Collection					
Space group	P2 ₁ 2 ₁ 2 ₁	P2 ₁ 2 ₁ 2 ₁	C2	C2	C2
Unit cell dimensions					
a, b, c (Å)	57.60, 66.34, 200.81	57.70, 66.14, 197.60	50.31, 82.49, 118.97	50.79, 82.00, 121.12	232.22, 63.10, 72.02
α, β, γ (°)	90.0	90.0	90.0, 92.4, 90.0	90.0, 90.1, 90.0	90.0, 91.72, 90.0
Wavelength (Å)	1.00000	0.97950 (<i>peak</i>)	1.00000	0.97890 (<i>peak</i>)	1.00000
Resolution (Å)	30.0 – 2.4	30.0 – 2.5	50.0 - 2.56	50.0 - 2.65	50.0 – 2.1
R_{sym}^b	5.6 (16.0)	6.9 (17.4)	4.1 (11.0) ^a	4.8 (19.1)	7.0 (21.3)
$I/\sigma(I)$	35.2 (5.9)	22.2 (3.9)	53.2 (10.5)	29.0 (2.8)	29.0 (4.2)
Completeness (%)	91.1(78.9)	81.3 (55.5)	93.2 (78.5)	91.7 (61.5)	93.3 (73.4)
Redundancy	8.4	3.9	5.7	2.7	5.1
Refinement					
Resolution (Å)	30 – 2.4		30 – 2.6		30 – 2.1
Number of reflections	25464		14269		57111
$R_{\text{work}}^c / R_{\text{free}}$	20.7 / 24.9		21.9 / 25.6		23.1 / 27.7
Number of atoms					
Protein	5264		2438		7384
Water	132		31		210
Rms deviations					
Bond lengths (Å)	0.0078		0.0072		0.0073
Bond angles (°)	1.2625		1.2252		1.1519

^aThe numbers in parentheses are statistics from the highest resolution shell.

^b $R_{\text{sym}} = \sum |I_{\text{obs}} - I_{\text{avg}}| / I_{\text{obs}}$, where I_{obs} is the observed intensity of individual reflection and I_{avg} is average over symmetry equivalents.

^c $R_{\text{work}} = \sum ||F_{\text{o}}| - |F_{\text{c}}|| / \sum |F_{\text{o}}|$, where $|F_{\text{o}}|$ and $|F_{\text{c}}|$ are the observed and calculated structure factor amplitudes, respectively. R_{free} was calculated with 5% of the data.